6164 J. Med. Chem. 2010, 53, 6164–6179
DOI: 10.1021/jm1005447

Journal of Medicinal Chemistry Article

Synthesis and Antiproliferative Evaluation of Certain Indeno[1,2-*c*]quinoline Derivatives. Part 2

Chih-Hua Tseng,[†] Cherng-Chyi Tzeng,[†] Chiao-Li Yang,[†] Pei-Jung Lu,[‡] Hui-Ling Chen,[‡] Hao-Yi Li,[§] You-Chung Chuang,[§] Chia-Ning Yang,*[,§] and Yeh-Long Chen*[,†]

[†]*Department of Medicinal and Applied Chemistry, College of Life Science, Kaohsiung Medical University, Kaohsiung City 807, Taiwan,* [‡]*Institute of Clinical Medicine, National Cheng-Kung University, School of Medicine, 138 Sheng-Li Road, Tainan 704, Taiwan, and* [§]*Institute of Biotechnology, National University of Kaohsiung, 700 Kaohsiung University Road, Kaohsiung, Taiwan*

Received May 5, 2010

Certain indeno[1,2-*c*]quinoline derivatives were synthesized and evaluated for their antiproliferation, DNA binding affinity, and topoisomerases (topo I and topo II) inhibitory activities. The preliminary results are the following: (1) substituent of the aminoalkoxyimino side chain at C_{11} is important for antiproliferative activities in which the terminal amine preferred to be a tertiary or the cyclic five-membered pyrrolidino ring; (2) among the indeno[1,2-*c*]quinoline derivatives evaluated, (*E*)-6-hydroxy-9-methoxy-11*H*-indeno[1,2-*c*]quinolin-11-one *O*-2-(pyrrolidin-1-yl)ethyl oxime (**8c**) was found to be one of the most cytotoxic agents with a GI_{50} value of 0.84, 0.89, and 0.79 μM against SAS, A549, and BT483, respectively, which is more active than camptothecin; (3) substituent at C_6 is crucial for the selective cytotoxicity in which the OH group is the most preferred while hydrogen or piperazine exhibited cytotoxicity on both cancer cells and Detroit-551; (4) a positive correlation of antiproliferative activity, DNA binding affinity, and topo I and topo II inhibitory activities has been observed for indeno[1,2-*c*]quinoline derivatives; (5) compound **8c** induced DNA fragmentation may through caspase-3 activation, phosphorylation of the histone protein H2AX at Ser139 (γ-H2AX), and PARP cleavage; (6) compound **8c** demonstrated significant tumor regression in the human breast xenograft model; (7) indeno[1,2-*c*]quinoline derivatives are a new class of molecules that have the potential to be developed as dual topo I and topo II inhibitory agents.

Introduction

DNA topoisomerases are nuclear enzymes that are involved in diverse cellular processes and therefore are important targets for several clinically used anticancer drugs. Topoisomerase I (topo I[a]) is the target for a series of camptothecin derivatives, while topoisomerase II (topo II) is the target for amsacrine (*m*-AMSA), etoposide, doxorubicin, and mitoxantrone. Currently, most of the topoisomerase inhibitors show selectivity against either topo I[1−9] or topo II[10−15] while only a small class of compounds is capable of inhibiting both enzymes.[16−21] Selective inhibition of the topo I enzyme can, however, induce a reactive increase in topo II levels and vice versa.[22] This mechanism is associated with the development of drug resistance. Searching for new compounds that inhibit both topo I and topo II is very important because of the deficiency of specific inhibitors to overcome multidrug resistance (MDR) cancer cells.

Amsacrine (*m*-AMSA), a 9-anilinoacridine derivative, has been clinically used for the treatment of leukemia and lymphoma because of its capability of intercalating DNA, leading to the inhibition of mammalian topo II.[23−26] Further structural modification has led to the discovery of improved broad spectrum anticancer agents that are capable of inhibiting the growth of certain solid tumors such as mammary adenocarcinoma, melanoma, and Lewis lung carcinoma.[27,28] These results prompted us to synthesize and evaluate 4-anilinofuro[2,3-*b*]quinoline derivatives which can be structurally related to 9-anilinoacridines by isosteric substitution of a benzene moiety for a furan ring.[29−34] Similar approaches to these compounds were also reported where the benzene moiety was isosterically replaced with a thiazole ring.[35,36]

Camptothecin (CPT,[37,38] Chart 1), an alkaloid isolated from *Camptotheca acuminata*, and its derivatives such as topotecan and irinotecan are prototypical topo I inhibitors and currently used as anticancer drugs. However, the chemically unstable lactone ring limited their clinical utility.[39,40] Recently, a number of indenoisoquinolines have been identified as novel topo I inhibitors with better pharmacokinetic features than CPT.[41−46] These compounds bind to a transient topo I−DNA covalent complex and inhibit the resealing of a single-strand nick that the enzyme creates to relieve superhelical tension in duplex DNA.[47−49] The indenoquinoline skeleton, which is known as the isosteric isomer of indenoisoquinoline, attracts only limited attention.[50−56] For example, certain indeno[1,2-*c*]quinolin-11-one scaffolds have been shown to possess antitumor activity.[51] The indeno[2,1-*c*]-quinoline **1** (TAS-103,[53−56] Chart 1) has been proved to be a novel topo I and topo II targeting agent that stabilizes cleavable complexes of topo−DNA at the cellular level.

*To whom correspondence should be addressed. or C.-N.Y.: phone, (886) 7-5919000, extension 7717; fax, (886)7-5919404; e-mail, cnyang@nuk.edu.tw. For Y.-L.C.: phone, (886) 7-3121101, ext 2684; fax, (886) 7-3125339; e-mail, yeloch@kmu.edu.tw.

[a] Abbreviations: topo I, topoisomerase I; topo II, topoisomerase II; MDR, multidrug resistance; CPT, camptothecin; MTT, microculture tetrazolium; GI_{50}, the concentration of 50% growth inhibition; SI, selective index; SAR, structure−activity relationship; Dox, doxorubicin; GOT, glutamic oxalacetic transaminase; GPT, glutamic pyruvic transaminase; BUN, blood urea nitrogen; PARP, poly ADP-ribose polymerase-1.

 Published on Web 07/28/2010

Chart 1. Structures of Camptothecin, Topotecan, Irinotecan, Indenoquinolinone **1**, Indenoquinolinone *O*-Alkyl Oxime **10b**, and Targeted Compounds

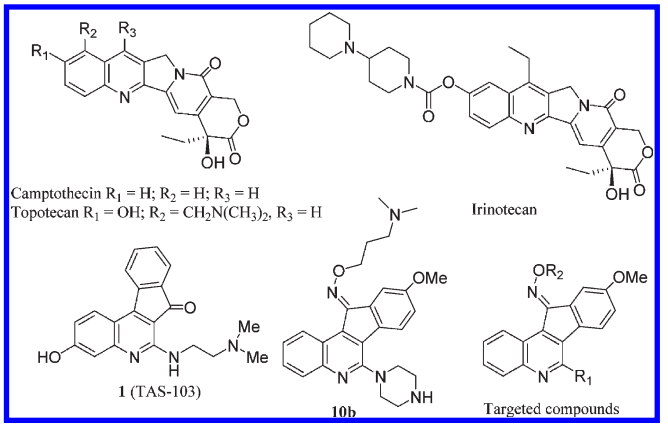

Scheme 1[a]

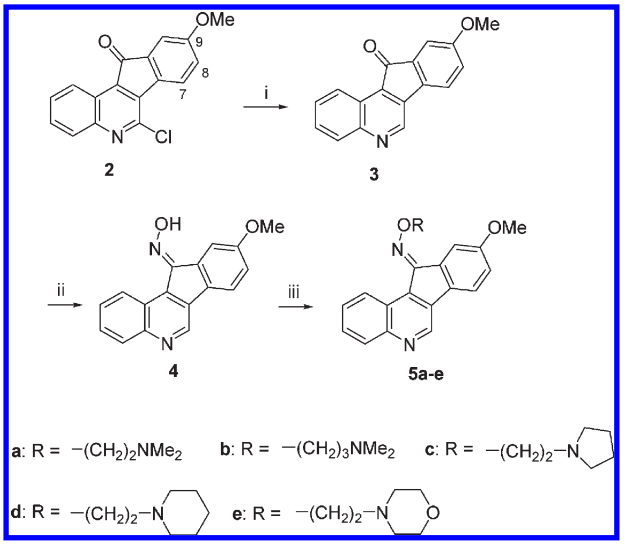

[a] Reagents and conditions: (i) Na, EtOH, reflux 48 h; (ii) $NH_2OH\cdot HCl$, ethoxyethanol, microwave (100 W), 30 min; (iii) NaH, alkyl halides, DMF, room temp, 2 h.

Recently, we have reported the synthesis and antiproliferative evaluation of certain indolo[2,3-*b*]quinoline[57,58] and indeno[1,2-*c*]quinoline derivatives.[59,60] Among them, 9-methoxy-6-(piperazin-1-yl)-11*H*-indeno[1,2-*c*]quinolin-11-one *O*-3-(dimethylamino)propyl oxime (**10b**,[59] Chart 1) was found to be more active than CPT against the growth of AGS and A549 with GI_{50} values of 6.84 and 0.38 μM, respectively.[59] The present report intends to establish the structure−activity relationships, concentrating on structural variations of the substituents on the indeno[1,2-*c*]quinoline pharmacophore, and to identify more potent and selective anticancer drug candidates. Because of the structural similarity of **10b** and **1**, the DNA binding affinity and the topo I and topo II inhibitory activities of these indeno[1,2-*c*]quinoline derivatives have also been evaluated.

Results and Discussion

Synthesis of Indeno[1,2-*c*]quinoline Derivatives. Reduction of 6-chloro-9-methoxy-11*H*-indeno[1,2-*c*]quinolin-11-one (**2**)[59] with Na/EtOH gave 9-methoxy-11*H*-indeno[1,2-*c*]quinolin-11-one (**3**) as described in Scheme 1. Treatment of **3** with hydroxylamine·HCl gave exclusively (*E*)-9-methoxy-11*H*-indeno[1,2-*c*]quinolin-11-one oxime (**4**) which was alkylated with 2-chloro-*N*,*N*-dimethylethanamine to give (*E*)-9-methoxy-11*H*-indeno[1,2-*c*]quinolin-11-one *O*-2-(dimethylamino)ethyl oxime (**5a**). The (*E*)-form configuration of the oxime moiety was unambiguously determined by the X-ray crystallography of **5a** (Figure 1; detailed parameters are included in the Supporting Information). Accordingly, compounds **5b**−**e** respectively were obtained by the treatment of **4** with the respective alkyl halides in a fairly good overall yield.

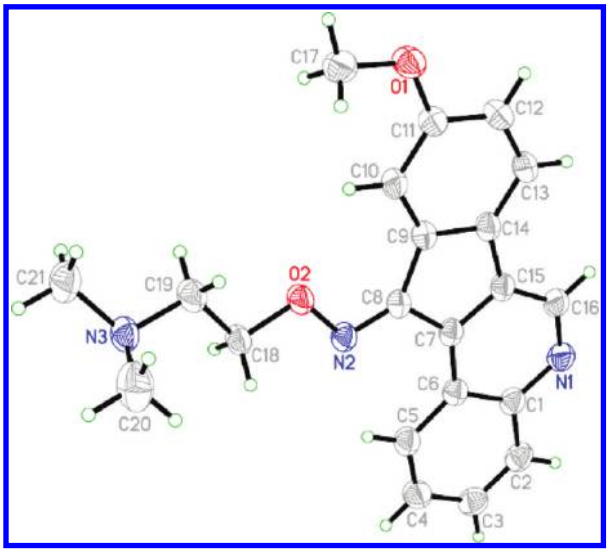

Figure 1. X-ray structure of compound **5a**.

The preparation of 6-hydroxy-9-methoxy-11*H*-indeno[1,2-*c*]quinolin-11-one alkyloximes **8a**−**e** and their 6-(piperazin-1-yl) counterparts **10a**−**e** is described in Scheme 2. Treatment of **2** with HCl gave 6-hydroxy-9-methoxy-11*H*-indeno[1,2-*c*]quinolin-11-one (**6**) which was then reacted with hydroxylamine·HCl to give exclusively (*E*)-6-hydroxy-9-methoxy-11*H*-indeno[1,2-*c*]quinolin-11-one oxime (**7**). Reaction of **6** with 2-*N*,*N*-dimethylaminoethoxyamine·HCl[61] in 2-ethoxyethanol gave exclusively (*E*)-6-hydroxy-9-methoxy-11*H*-indeno[1,2-*c*]quinolin-11-one *O*-2-(dimethylamino)ethyl oxime (**8a**) in 81% yield. The (*E*)-form aminoalkylated oxime derivatives **8b**−**e** were obtained by the treatment of **6** with the respective alkoxyamines. Accordingly, 9-methoxy-6-(piperazin-1-yl)-11*H*-indeno[1,2-*c*]quinolin-11-one *O*-2-(pyrrolidin-1-yl)ethyl oxime (**10c**) was prepared from **9** by the treatment with 1-(2-chloroethyl)-pyrrolidine·HCl. Preparation of compounds **10a**, **10b**, **10d**, and **10e** had been described in our previous report.[59]

Antiproliferative Activities. All the synthesized indeno[1,2-*c*]quinoline derivatives were evaluated in vitro against a panel of five cancer cell lines including human cervical epithelioid carcinoma (HeLa), oral squamous cell carcinoma (SAS), non-small-cell lung cancer (A549), prostate cancer (PC-3), and hepatocelluar carcinoma (SKHep), using microculture tetrazolium (MTT, 3-[4,5-dimethylthiazol-2-yl]-2,5-diphenyltetrazolium bromide) assay. The skin Detroit-551 normal fibroblast cells were also evaluated, since a potential anticancer drug candidate should selectively affect only tumor cells and not somatic cells. The concentration that inhibited the growth of 50% of cells (GI_{50}) was determined from the linear portion of the curve by calculating the concentration of agent that reduced absorbance in treated cells, compared to control cells, by 50%. The GI_{50} results of 11*H*-indeno[1,2-*c*]quinoline-11-one derivatives are summarized in Table 1. The C_{11}-hydroxyimino

Scheme 2[a]

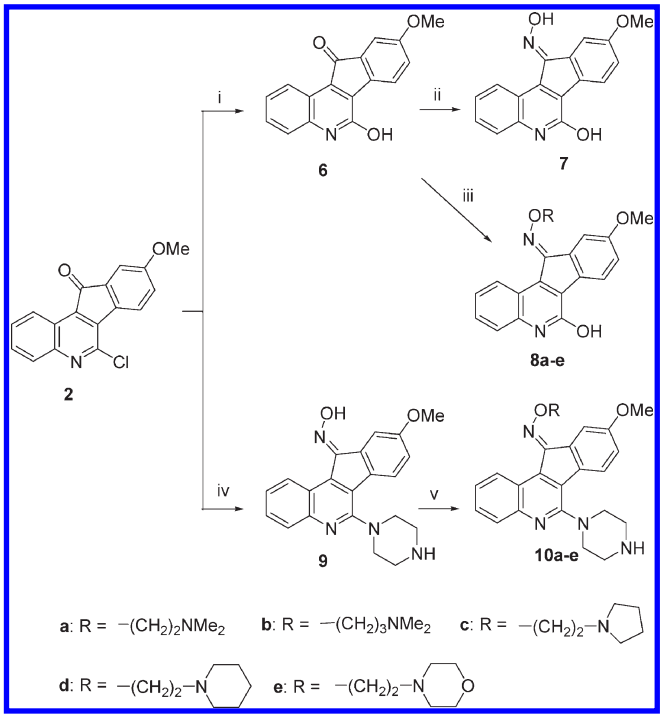

[a] Reagents and conditions: (i) 36% HCl, DMF, reflux 2 h; (ii) $NH_2OH \cdot HCl$, ethoxyethanol, microwave (100 W), 30 min; (iii) $NH_2OR \cdot HCl$, ethoxyethanol, reflux 2 h; (iv) (a) piperazine, ethoxyethanol in sealed tube, 200 °C, 48 h; (b) $NH_2OH \cdot HCl$, ethoxyethanol, microwave (100 W), 30 min; (v) NaH, alkyl halides, DMF, room temp, 2 h.

derivative **4** is more active than its carbonyl precursor **3** with the exception of A549, in which compound **3** is fairly active with a GI_{50} value of 13.50 μM. Introduction of an aminoalkyl side chain on the C_{11}-hydroxyimino moiety improves antiproliferative activities (**5a** > **4**). For the C_6-unsubstituted indeno[1,2-*c*]quinolines **5a**−**e**, the *O*-2-(dimethylamino)ethyl oxime **5a** is more active then its *O*-3-(dimethylamino)propyl oxime counterpart **5b** against HeLa, SAS, and PC-3. Comparable activities of **5a** vs **5c** indicated that the terminal aminoalkyl side chain can be a tertiary amine or the cyclic five-membered pyrrolidino ring. However, the cyclic six-membered rings such as piperidino and morpholino are unfavorable in which the antiproliferative activities decreased in the order of **5c** > **5d** > **5e**. Among these cancer cells evaluated, HeLa cell is the most susceptible. Compounds **5a** and **5c** were found to exhibit better selective cytotoxicities than CPT. The selective index (SI), defined as GI_{50} of Detroit-551/GI_{50} of HeLa cell, for **5a** and **5c** is 16.31 and 13.98, respectively, while the SI for CPT is 5.50. Compounds **5a** and **5c** are not only more selective but also more active than CPT against the growth of SAS and A549 cancer cells. The SI values for CPT against SAS and A549 are 0.17 and 0.35, respectively, while the SI values for **5a** and **5c** are about 4.08 and 6.01. The structure−activity relationships (SAR) obtained from C_6-unsubstituted indeno[1,2-*c*]quinolines **5a**−**e** can also be applied for their C_6−OH derivatives **8a**−**e**. Thus, compounds **8a**, **8b**, and **8c**, which are approximately equipotent, are more active than **8d** which in turn is more active than **8e**. Compound **8c** exhibited very potent antiproliferative activities against HeLa, SAS, and A549 with GI_{50} of 0.23, 0.84, and 0.89 μM, respectively, which are equally active or more active than CPT. Although compounds **8a** and **8c** are highly cytotoxic on cancer cells, they are only weakly active against the growth of Detroit-551 normal fibroblast cells with GI_{50} of 9.60 and 12.44 μM, respectively. The SI for **8a** and **8c** is 41.74 and 54.09, respectively, indicating their high potential for further development.

The comparable antiproliferative activities were observed for the C_6-OH derivatives **8a**−**e** and their respective C_6-piperazine counterpart **10a**−**e**.[59] However, **10a**−**e** are highly cytotoxic against the growth of Detroit-551 with GI_{50} in a range 1.47−2.77 μM. The SI for C_6-piperazine derivative **10a**−**e** is much lower than that of their respective C_6-OH counterpart **8a**−**e**.

The antiproliferative activities for the *N*,*N*-dimethylaminoethyl derivatives against the growth of HeLa cell decreased in the order of the C_6-OH indeno[1,2-*c*]quinoline **8a** (GI_{50} = 0.23 μM) > C_6-unsubstituted derivative **5a** (GI_{50} = 0.42 μM) > C_6-piperazine counterpart **10a** (GI_{50} = 0.92 μM). However, the cytotoxicity against the growth of Detroit-551 decreased in the order of **10a** (GI_{50} = 2.72 μM) > **5a** (GI_{50} = 6.85 μM) > **8a** (GI_{50} = 9.60 μM). The SI for the C_6-OH indeno[1,2-*c*]quinoline **8a** is 41.74, which is more selective than the C_6-unsubstituted derivative **5a** (SI = 16.31) and the C_6-piperazine derivative **10a** (SI = 2.96). The same SAR was observed for the pyrrolidin-1-ylethyl derivatives in which the antiproliferative activities against the growth of HeLa cell decreased in the order of **8c** > **5c** > **10c**, while the cytotoxicity against the growth of Detroit-551 decreased in the order of **10c** > **5c** > **8c**. The SI for the C_6-OH indeno[1,2-*c*]quinoline **8c** is 54.09, which is more selective than the C_6-unsubstituted derivative **5c** (SI = 13.98) and the C_6-piperazine derivative **10c** (SI = 2.58). Compound **8c** can strongly inhibit not only the growth of HeLa cell but also the growth of SAS, A549, and BT483 with a GI_{50} of 0.84, 0.89, and 0.79 μM, respectively, which is more active than the positive CPT.

Topoisomerases Assay. The DNA binding affinity and topo I and topo II inhibitory activities of these indeno[1,2-*c*]-quinoline derivatives are summarized in Table 2. For the C_6-unsubstituted indeno[1,2-*c*]quinolines **5a**−**e**, good correlations have been observed for cytotoxicity, DNA binding affinity, and topo I and topo II inhibitory activities. The more cytotoxic *O*-2-(dimethylamino)ethyl oxime **5a** and *O*-2-(pyrrolidin-1-yl)ethyl oxime **5c** exhibited fairly good DNA binding affinities and topoisomerases inhibitory activities while less cytotoxic *O*-2-(piperdin-1-yl)ethyl oxime **5d** demonstrated only a weak DNA affinity and weak topoisomerases inhibitory activities. The noncytotoxic *O*-2-morpholinoethyl oxime **5e** has neither DNA affinity nor topoisomerases inhibitory activities. Compound **5a** exhibited a dual inhibitory activity on topo I and topo II with an IC_{50} value of 7.20 and 6.70 μM, respectively, while the positive CPT was inactive against topo II with an IC_{50} value of > 100 μM. Comparable topoisomerases inhibitory activities of **5a** and **5c** indicated that the terminal moiety can be a tertiary amine or the cyclic five-membered pyrrolidino ring. However, the cyclic six-membered rings such as piperidino and morpholino are unfavorable in which topoisomerases inhibitory activities decreased in the order of **5c** > **5d** > **5e**. Although compound **5b** has no DNA binding affinity, it possesses weak topoisomerases inhibitory activities. A similar SAR was observed with C_6-OH derivatives **8a**−**e** in which the highly cytotoxic **8a** and **8c** exhibited the strongest DNA binding affinity and potent topoisomerases inhibitory activities with an IC_{50} value of 7.40 and 3.76 μM, respectively, against topo I and 10.25 and 8.26 μM, respectively, against topo II. Compound **8b**, which binds with DNA in a moderate

Table 1. Antiproliferative Activities of Indeno[1,2-*c*]quinoline Derivatives

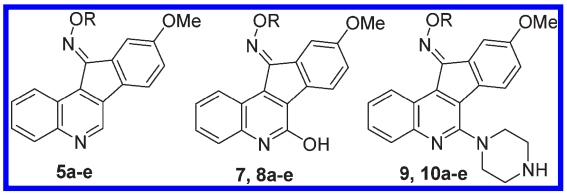

	R	GI_{50} (μM) / selective index (SI[a])						
		HeLa	SAS	A549	PC-3	SKHep	BT483	Detroit 551
CPT		0.18 ± 0.10 (5.5)	6.00 ± 2.70 (0.17)	2.80 ± 0.70 (0.35)	0.09 ± 0.02 (11)	0.22 ± 0.13 (4.5)	1.03 ± 0.25 (0.96)	0.99 ± 0.09
3		17.21 ± 1.69 -	> 30	13.50 ± 4.70 -	> 30	> 30	> 30	nd
4		11.40 ± 3.08	> 30	> 30	> 30	8.42 ± 0.38 -	> 30	nd
5a	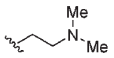	0.42 ± 0.04 (16.31)	1.14 ± 0.02 (6.01)	1.30 ± 0.15 (5.27)	1.89 ± 0.33 (3.62)	1.20 ± 0.24 (5.71)	3.61 ± 1.30 (1.90)	6.85 ± 0.57
5b	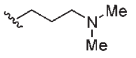	1.11 ± 0.47 (3.11)	6.10 ± 0.90 (0.57)	1.83 ± 1.40 (1.89)	5.65 ± 0.31 (0.61)	1.07 ± 0.51 (3.22)	0.93 ± 0.16 (3.71)	3.45 ± 0.21
5c	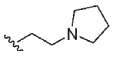	0.45 ± 0.02 (13.98)	1.19 ± 0.20 (5.29)	1.54 ± 0.38 (4.08)	2.32 ± 0.52 (2.71)	1.51 ± 0.31 (4.17)	3.11 ± 0.37 (2.02)	6.29 ± 0.57
5d	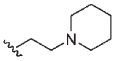	2.67 ± 0.65 (2.36)	7.18 ± 0.07 (0.88)	8.48 ± 1.82 (0.74)	6.38 ± 2.76 ((0.99)	5.26 ± 2.05 (1.20)	5.17 ± 0.32 (1.22)	6.30 ± 0.34
5e	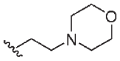	16.93 ± 3.80 -	15.72 ± 1.40 -	28.25 ± 4.12 -	7.81 ± 2.81 -	20.76 ± 4.62 -	10.19 ± 3.24 -	nd
8a	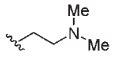	0.23 ± 0.02 (41.74)	1.10 ± 0.09 (8.73)	1.00 ± 0.03 (9.60)	5.34 ± 2.17 (1.80)	2.56 ± 0.53 (3.75)	4.04 ± 0.52 (2.38)	9.60 ± 0.92
8b	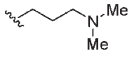	0.20 ± 0.08 (10.45)	3.10 ± 0.20 (0.67)	0.63 ± 0.06 (3.32)	4.35 ± 0.90 (0.48)	0.75 ± 0.20 (2.79)	1.29 ± 0.24 (1.62)	2.09 ± 0.30
8c	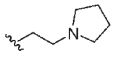	0.23 ± 0.02 (54.09)	0.84 ± 0.05 (14.81)	0.89 ± 0.08 (13.98)	1.83 ± 0.78 (6.80)	1.24 ± 0.32 (10.03)	0.79 ± 0.13 (15.75)	12.44 ± 0.51
8d	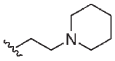	0.84 ± 0.10 (8.93)	5.39 ± 0.78 (1.39)	6.95 ± 1.73 (1.08)	5.74 ± 3.88 (1.31)	4.28 ± 1.27 (1.75)	1.59 ± 0.64 (4.72)	7.50 ± 0.47
8e	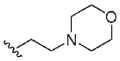	5.02 ± 0.84 -	16.52 ± 2.46 -	> 30	13.62 ± 2.53 -	10.37 ± 1.86 -	6.04 ± 0.66 -	nd
9	H	2.35 ± 0.25 -	6.10 ± 0.90 -	3.80 ± 0.85 -	4.86 ± 2.03 -	3.75 ± 1.28 -	- -	nd
10a	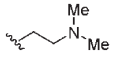	0.92 ± 0.38 (2.96)	6.33 ± 0.86 (0.43)	0.71 ± 0.12 (3.83)	4.61 ± 1.18 (0.59)	3.01 ± 2.18 (0.90)	1.10 ± 0.21 (2.47)	2.72 ± 0.31
10b	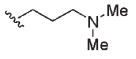	0.37 ± 0.06 (7.49)	4.93 ± 0.57 (0.56)	0.38 ± 0.21 (7.29)	5.28 ±0.67 (0.52)	2.95 ±2.10 (0.94)	1.37 ± 0.26 (2.02)	2.77 ± 0.16
10c	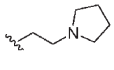	0.57 ± 0.21 (2.58)	2.43 ±1.28 (0.60)	0.50 ± 0.20 (4.63)	3.37 ± 1.18 (0.44)	0.68 ±0.30 (2.16)	1.43 ± 0.23 (1.03)	1.47 ± 0.28
10d	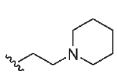	0.78 ± 0.22 (2.95)	5.81 ± 0.48 (0.40)	0.87 ± 0.12 (2.64)	5.62 ± 0.48 (0.41)	1.57 ± 0.42 (1.46)	4.03 ± 0.57 (0.57)	2.30 ± 0.10
10e	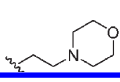	0.78 ± 0.20 (3.33)	6.93 ± 1.31 (0.38)	2.20 ± 0.17 (1.18)	6.47 ± 0.91 (0.40)	0.98 ± 0.27 (2.65)	3.75± 0.60 (0.69)	2.60 ± 0.14

[a] SI: selectivity index = (GI_{50} of Detroit-551)/(GI_{50} of cancer cell line).

Table 2. DNA Binding Affinity and Topoisomerases (topo I and topo II) Inhibitory Activities of Indeno[1,2-*c*]quinoline Derivatives

Compd.	R	DNA bindig affinity	Topo I inhibition at 10 μM (%)	IC_{50} μM (topo I)	Topo II inhibition at 10 μM (%)	IC_{50} μM (topo II)
CPT[a]		nd	85	2.2	0	>100
Dox[b]		nd	35	20	85	1.9
3		nd	0	> 100	0	>100
4		nd	nd	nd	nd	nd
5a	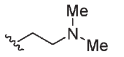	++	82	7.2	75	6.70
5b	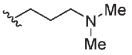	-	5	40	75	13.15
5c	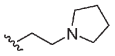	++	67	8.2	80	6.50
5d	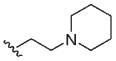	+	28	16.5	50	10.05
5e	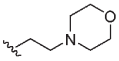	-	0	> 100	0	>100
8a	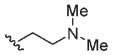	+++	73	7.4	46	10.25
8b	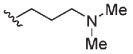	++	3	> 100	77	7.14
8c	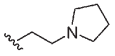	+++	71	3.76	60	8.26
8d	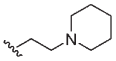	+/-	0	> 100	0	>100
8e	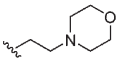	-	0	> 100	0	>100
10a	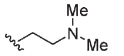	++	56	8.5	75	4.87
10b	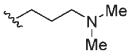	++	70	6.6	88	4.05
10c	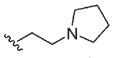	++	48	12.8	74	6.44
10d	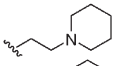	+	45	11.5	68	8.00
10e	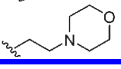	nd	40	13.0	100	5.97

[a] CPT: camptothecin. [b] Dox: doxorubicin.

affinity, is inactive in the inhibition of topo I activity. However, Compound **8b** exhibited potent inhibitory activity on topo II with an IC_{50} value of 7.14 μM. For C_6-piperazine derivatives **10a**−**c**, good correlations have been observed for cytotoxicity, DNA binding affinity, and topoisomerases inhibitory activities. For example, highly cytotoxic **10a**, which exhibited a strong DNA binding affinity, was demonstrated to possess potent topo I and topo II inhibitory activities with an IC_{50} value of 8.50 and 4.87 μM, respectively. Comparable antiproliferative activity, DNA binding affinity, and topoisomerases exhibited by **10a**, **10b**, and **10c** indicated that the terminal aminoalkyl side chain can be a tertiary amine or the cyclic five-membered pyrrolidino ring. However, the cyclic six-membered piperidino and morpholino derivatives **10d** and **10e**, respectively, which exhibited potent antiproliferative and topoisomerases inhibitory activities, were only weakly active or inactive to bind with DNA. Among these indeno[1,2-*c*]quinoline derivatives evaluated, compounds **5a**, **5c**, **8a**, **8c**, **10a**, **10b**, and **10c** are potential leads that possess potent antiproliferative activity, DNA binding affinity, and topoisomerases inhibitory activities. We decided to select compound **8c** for further mechanism study because it showed the lowest cytotoxicity against the growth of Detroit-551 normal fibroblast cells with GI_{50} of 12.44 μM. The results in Figure 2A showed that **8c** is a potent topo I inhibitor, since the inhibitory DNA pattern by 1 μM of **8c** is similar to that by 50 μM CPT, a known topo I inhibitor. The topo I inhibitory activity of **8c** is in a dose dependent manner (Figure 2A). Our results have also indicated that compounds **5a**, **5c**, and **8c** are more potent topo II inhibitors than the positive doxorubicin (Dox) at 10 μM (Figure 2B). Therefore, compound **8c** has been proved to possess dual inhibitory activities against both topo I and topo II and the inhibitory activities contribute to the cell proliferation inhibition and GI_{50} values (Table 1).

DNA Fragmentation and Apotosis in BT483 Cells. Compound **8c** can effectively inhibit the BT483 proliferation with a GI_{50} value of 0.79 μM, and an SI of 15.75 prompts us to examine whether **8c** can induce cancer cell death. We first used flow cytometric analysis to investigate the effect of **8c** on the cell cycle progression and cell death. Cells accumulated in sub-G1 phase exhibited DNA fragmentation and cell death. Figure 3A showed that the sub-G1 population increased from 1% of DMSO control group to 43%, 58%, and 88% for 1.0, 3.0, and 10.0 μM, respectively. The DNA fragmentation was also observed in **8c** treated BT483 cells in DAPI

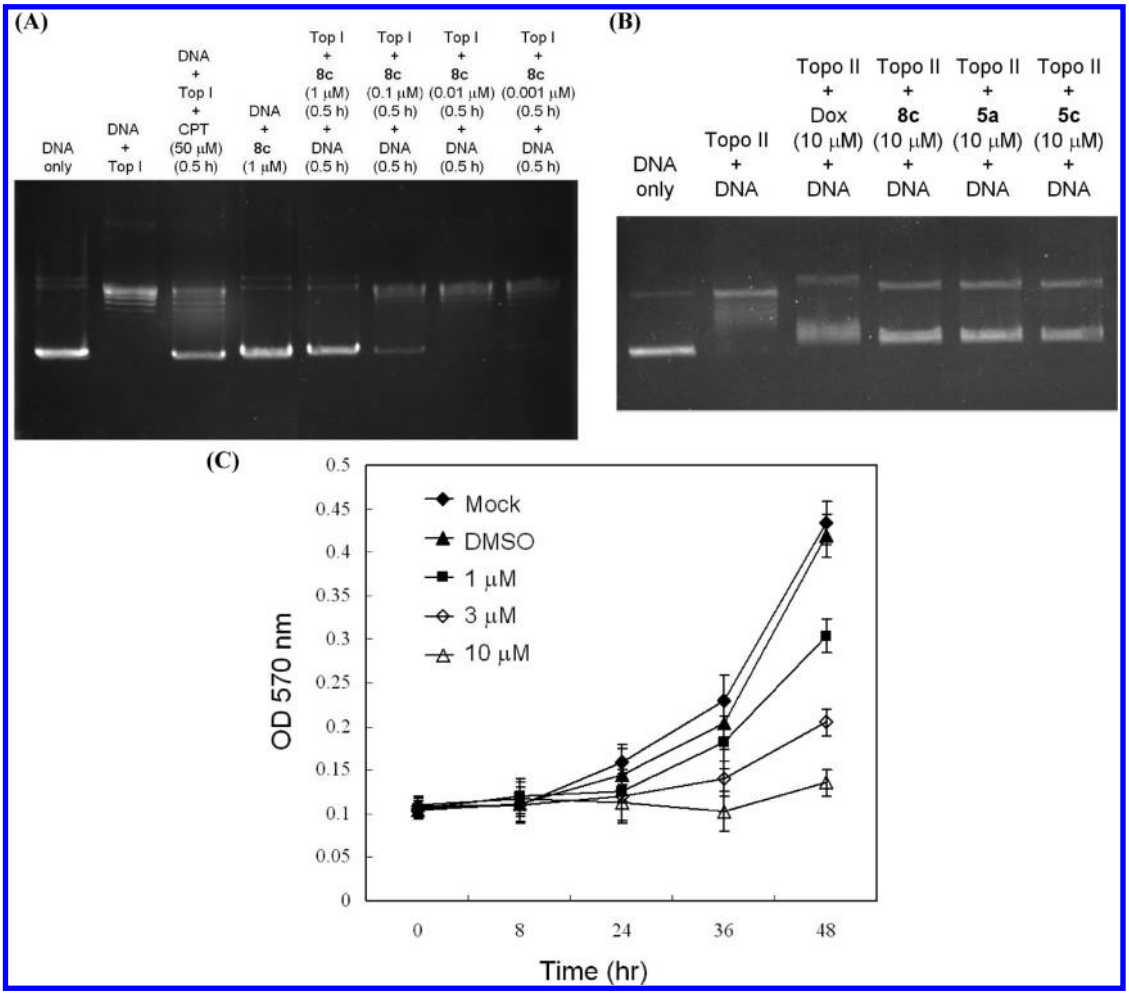

Figure 2. (A) Inhibition of human topoisomerase I (topo I) relaxation activities of indeno[1,2-*c*]quinoline derivatives, showing preincubation of topo I with compound **8c** and camptothecin (CPT) followed by addition of supercoiled pBR322 DNA: lane 1, supercoiled pBR322 DNA alone; lane 2, same as lane 1 but DNA was added after preincubation of topo I with reaction buffer and with 0.5% DMSO, respectively, for 30 min at 37 °C; lane 3, preincubated with CPT (50 μM); lane 4, only supercoiled DNA incubated with compound **8c**; lanes 5−8, supercoiled DNA was incubated with topo I and various concentrations of compound **8c** as indicated. Reactions were stopped by addition of SDS to a final concentration of 0.5% (w/v), and samples were electrophoresed in 1% agarose gel. Positions of supercoiled DNA (low) and relaxed DNA (high) are indicated. (B) Inhibition of human topoisomerase II (topo II) relaxation activities of indeno[1,2-*c*]quinoline derivatives, showing preincubation of topo II with compounds **5a**, **5c**, **8c**, and doxorubicin (Dox) followed by addition of supercoiled pBR322 DNA: lane 1, supercoiled pBR322 DNA alone; lane 2, same as lane 1 but DNA was added after preincubation of topo II with reaction buffer and with 0.5% DMSO, respectively, for 30 min at 37 °C; lane 3, preincubated with Dox (10 μM); lane 4, only supercoiled DNA incubated with compound **8c**; lanes 5 and 6, supercoiled DNA was incubated with topo II and the concentrations of compounds **5a** or **5c** as indicated. (C) Antiproliferative effects of **8c** on breast cancer BT483 cell. Adherent cells that proliferated in 96-well plates (10^4 cells/well) were incubated with different concentrations of **8c** (1.0, 3.0, and 10 μM), respectively, and determined by MTT assay at various time intervals.

staining experiment (Figure 3B). Compound **8c** induced DNA fragmentation was also confirmed by the DNA ladder analysis that only the **8c** treated cell showed the DNA ladder but not the DMSO control or MOCK group (Figure 3C). The results of **8c** induced DNA fragmentation in DNA ladder analysis are consistent with the results using flow cytometry assay (Figure 3A). Moreover, immunoblotting analysis was performed to support this conclusion by showing **8c** induced phosphorylation of the histone protein H2AX at Ser139 (γ-H2AX) (Figure 3D), which is a major response to DNA damage. Finally, our results suggested that compound **8c** induced DNA fragmentation may be through the caspase-3 activation and PARP cleavage (Figure 3D).

3D-QSAR Model for Antiproliferative Activity. 3D-QSAR analysis was performed by Sybyl 8.1 (Tripos International, 1699 South Hanley Road, St. Louis, MO 63144) to investigate how the substituents of indeno[1,2-*c*]quinoline derivatives influence the inhibitory activities against HeLa cell growth and to provide guidelines for future synthesis. Restricted to the small size of our data set, except compounds **6** and **7** without GI_{50} values, 18 compounds were all included to build a CoMFA model. The 18 studied structures with charge assignment done with Gasteiger−Marsili method were generated for CoMFA analysis by applying 100 steps in steepest descent algorithm followed by 500 steps in conjugate gradient algorithm for geometry minimization without constraints on the internal geometry of the molecules. We assumed that each compound would adopt a conformation in its lowest energy and used database alignment protocol in Sybyl 8.0 to pairwise align the structures according to the core conformational template specified in ball and stick as shown in Figure 4. To build the CoMFA model, the CoMFA descriptors and steric (Lennard-Jones 6−12 potential) and electrostatic (Coulombic potential) field energies are calculated with a sp^3 carbon atom carrying a +1.0 charge to serve as a probe atom

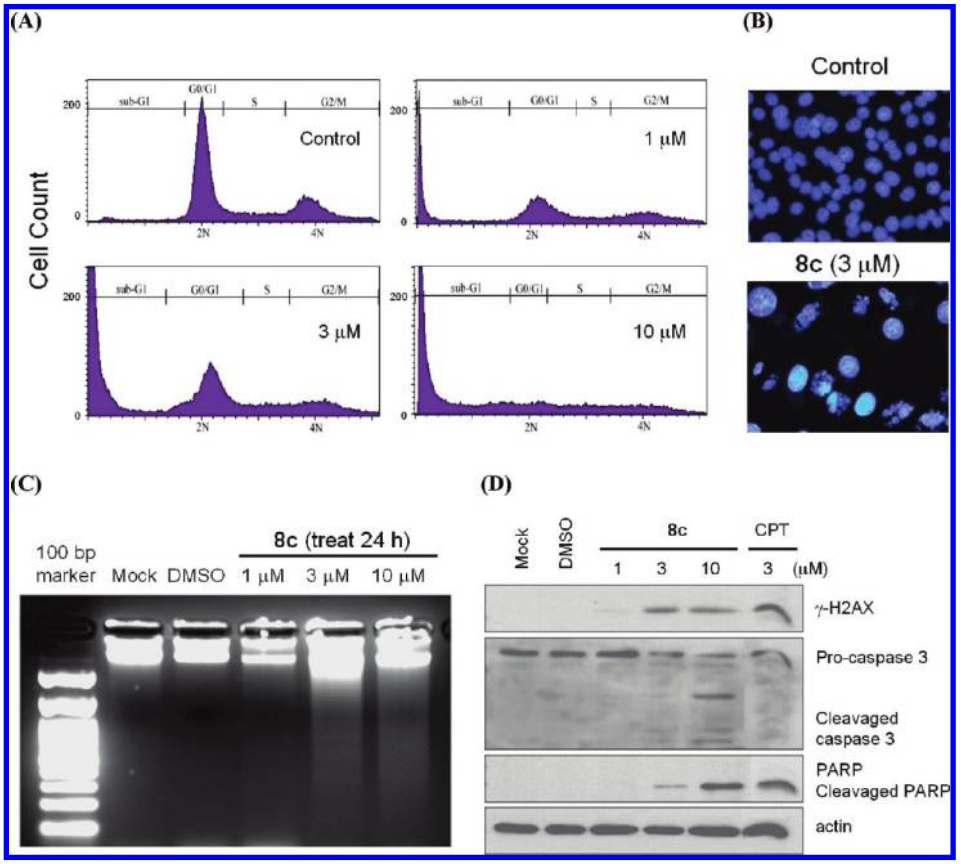

Figure 3. (A) Compound **8c** induced sub-G1 cell population in a dose-dependent manner. Flow cytometry was used to measure the DNA content and the cell-cycle phase of propidium iodide-stained cells. G1, S, and G2/M are phases of the cell cycle. Sub-G1 events correspond to cells or cell fragments with a lower DNA content and are indicative of apoptosis. Cells were treated with 0 (controls), 1, 3, and 10 μM **8c** for 24 and 48 h. The vertical axes indicate cell counts, and horizontal axes indicate DNA content; 2n and 4n are positions for G1 and G2/M populations, respectively. Percentage of cells was estimated by the computer program installed in the flow cytometry instrument (FACScan, Becton Dickinson). (B) DAPI staining showed that the nuclei of BT483 cells became fragmented and giant. Breast cancer BT483 cells were treated for 24 h with 3 μM **8c**, fixed, and stained with 4′-6-diamidino-2-phenylindole (DAPI) as described (Experimental Section) before mounting. Fluorescence microscopy was carried out (Olympus LX71 inverted microscope, 10× objective), and representative images were taken. (C) DNA ladder experiment showing that the DNA fragmentation was induced by **8c** treatment for 24 h in a dose dependent manner. (D) Apoptosis was induced after the BT483 cells had been treated for 24 h with **8c** at the indicated concentrations. Compound **8c** activated caspase-3 and induced PARP cleavage and H2AX phosphorylation in BT483 cells. Analysis of the expression of proteins in the lysates of treated and untreated cells was carried out by SDS−PAGE and Western blot analysis as described (Experimental Section). Primary antibodies against procaspase-3, inactivated/cleaved PARP, and phosphohistone H2AX (Ser139) were used. As an internal standard for equal loading, the blots were probed with an anti-β-actin antibody. M: mock. D: DMSO. CPT was used as a positive control.

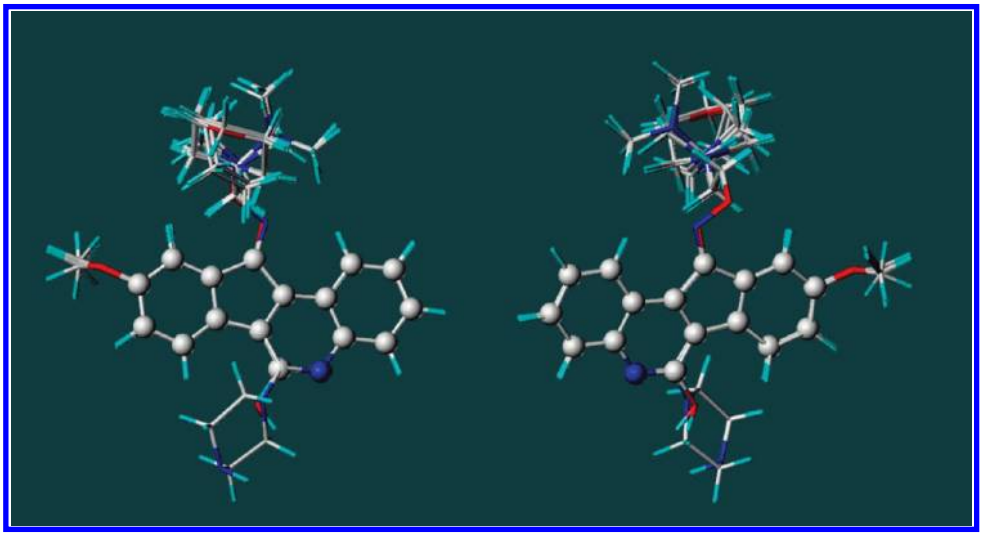

Figure 4. Different views of the aligned 18 compounds. The core used in the alignment protocol of the Sybyl 8.1 program is specified in ball and stick.

Table 3. Experimental and 3D-QSAR Predicted pGI_{50} Values and Statistical Results of CoMFA Models

compd	exptl pGI_{50}	predicted pGI_{50}, training set	residuals
3	4.76	4.62	0.14
4	4.94	4.94	0.01
5a	6.38	6.18	0.20
5b	5.95	6.10	−0.15
5c	6.35	6.34	0.01
5d	5.57	5.62	−0.05
5e	4.77	5.10	−0.33
6	NA[a]		
7	NA[a]		
8a	6.64	6.57	0.07
8b	6.70	6.49	0.21
8c	6.64	6.72	−0.08
8d	6.08	5.99	0.09
8e	5.30	5.49	−0.19
9	5.63	5.66	−0.03
10a	6.04	6.42	−0.38
10b	6.43	6.30	0.13
10c	6.24	6.46	−0.22
10d	6.11	5.89	0.22
10e	6.11	5.77	0.34

parameter	value
q^{2} [b]	0.635
ONC[c]	4
SEE[d]	0.227
R^2	0.901
F	29.477
fraction	
steric	0.618
electrostatic	0.3382

[a] NA: not available. [b] q^2: cross-validated R^2. [c] ONC: optimal number of components. [d] SEE: standard error.

using Sybyl default parameters. The statistical results are listed in Table 3. The optimal number of components (ONC = 4) was recommended after a satisfactory leave-one-out cross-validated run with $q^2 = 0.635$. Generally a q^2 value larger than 0.5 indicates that the model is internally predictive and the future model built without cross-validation shall be accountable. The final model and coefficients such as R^2 and F were obtained by using the optimal number of components and all the data points in the training set. Note that the resulting $R^2 = 0.901$ is larger than the criterion value of 0.6 for a fairly good model.

Shown in Figure 5 is the graph of the actual pGI_{50} versus the predictions. All the points in this plot fall within 0.5 logarithmic units. Shown in Figure 6 are the stdev*coefficient contour maps of steric and electrostatic fields generated by the CoMFA model with the training set. In Figure 6, the green regions are sterically favorable while the yellow regions are sterically unfavorable. The red regions in the electrostatic field are negative charge favorable, while the blue regions are positive charge favorable. In Figure 6A a big green contour is located in the side chain extending from position C_{11}, and this explains why **3** has a very small pGI_{50} (4.76). Beyond this green contour is a yellow contour which indicates that a bulky end moiety of the chain reduces the inhibition. Accordingly, comparison of compounds **5a**, **5c**, and **5d** shows declining pGI_{50} values 6.38, 6.35, and 5.57. Compounds **8b**, **8c**, and **8d** also follow the same trend. A tiny green contour located around position C_6 suggests that a hydroxyl group is better than a hydrogen atom. Therefore, compounds **8e**, **8a**, **8b**, **8c**, and **8d** are better than their counterpart compounds **5e**, **5a**, **5b**, **5c**, and **5d**, respectively. A blue contour located at

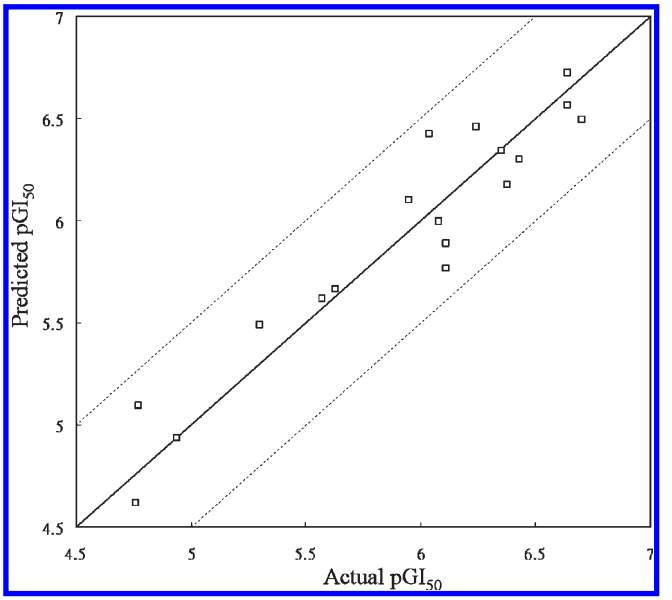

Figure 5. CoMFA predictions for the training set for pGI_{50} of the HeLa cell line.

the end of the above-mentioned side chain (Figure 6B) indicates that placing a negatively charged atom would decrease the activity. This explains why compound **5e** is less active than compound **5d**.

On the basis of the field analysis, guidelines are made to design potent indeno[1,2-*c*]quinoline derivatives against HeLa cell growth: (1) including an extended chain on position C_{11} is necessary; (2) if there is a ring moiety in the end of the chain, the optimal ring size is 5 and the ring should not include any negatively charged atom; (3) a hydroxyl group at position C_6 is better than a hydrogen atom.

Pharmacokinetic Evaluation. The pharmacokinetic parameters are summarized in Table 4 for intravenous and oral administration. The mean plasma concentration−time profiles are shown in Figure 7. Following an intravenous dosing, **8c** showed high systemic clearance (CL = 193 mL/(min·kg)) and high volume of distribution at steady state (V_{ss} = 12.3 L/kg) (Table 4). The AUC of **8c** was low (172 ng·h/mL), likely due to its high systemic clearance. Following a single intravenous dosing, **8c** showed short mean residence time (MRT = 1.1 h) and short terminal half-life (1.5 h). At an oral dose of 20 mg/kg, **8c** showed rapid oral absorption in mice, with a short T_{max} of 1.0 h. The drug exposure was poor, and the mean C_{max} and AUC of **8c** were 63 ng/mL and 187 ng·h/mL, respectively. Oral bioavailability of **8c** was 10.9%. The mean residence time (MRT) and the terminal half-life ($t_{1/2}$) were 3.4 and 2.2 h, respectively.

Xenographic Studies of Human Breast Cancer. The anticancer effect of **8c** in a human breast cancer xenograft nude mice model was then used to evaluate whether **8c** is a potential candidate against breast cancer cell growth in vivo. A single cell suspension of 2×10^5 BT483 cells was inoculated subcutaneously *into* the dorsum of each nude mice. Intraperitoneal administration (ip) of **8c** was carried out in nude mice 7 days after the inoculation that tumor size approximately reached 5 mm^3. Compound **8c** was administered twice on the 14th day and 28th day at the peritumoral region, and the final drug administration concentration was 10 and 20 mg/kg, respectively. As shown in Figure 8A, the average tumor size of both 10 and 20 mg/kg of **8c** treated groups was

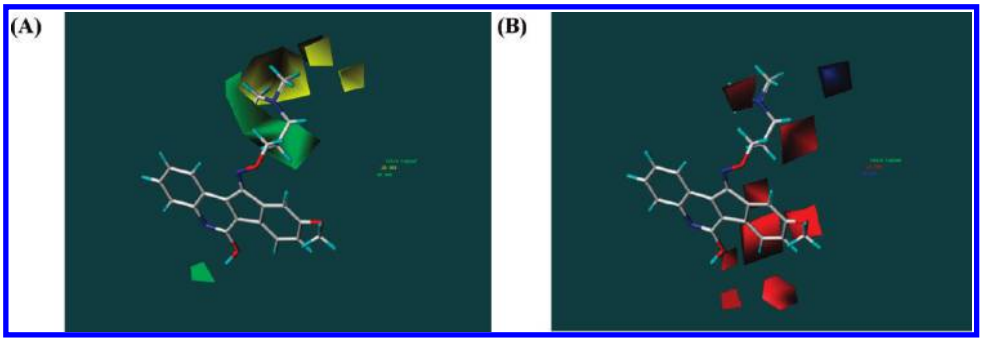

Figure 6. (A) Steric fields generated with the CoMFA model with training set data. Yellow indicates regions where bulky groups decrease activity (contribution level of 80%), whereas green indicates regions where bulky groups increase activity (contribution level of 20%). (B) Electrostatic fields generated with the CoMFA model with training set data. Red indicates regions where negatively charged groups increase activity (contribution level of 15%), whereas blue indicates regions where positively charged groups increase activity (contribution level of 80%).

Table 4. Pharmacokinetic Parameters of **8c** in Fasted Male CD-1 (Crl.) Mice

intravenous dosing at 2.0 mg/kg		oral dosing at 20 mg/kg	
PK parameter	mean	PK parameter	mean
$AUC_{(0-inf)}$ (ng·h/mL)	172	C_{max} (ng/mL)	63
MRT (h)	1.1	$AUC_{(0-inf)}$ (ng·h/mL)	187
CL (mL/(min·kg))	193	T_{max} (h)	1.0
V_{ss} (L/kg)	12.3	MRT (h)	3.4
V_z (L/kg)	25.5	$t_{1/2}$ (h)	2.2
$t_{1/2}$ (h)	1.5	bioavailability (%)	10.9

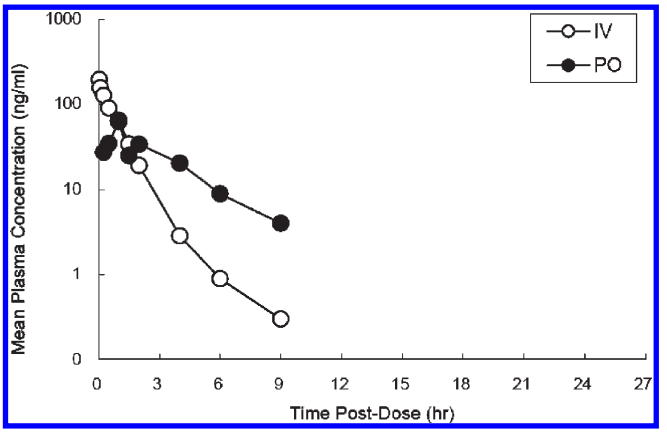

Figure 7. Mean plasma concentration−time profiles of **8c** in male CD-1 (Crl.) mice following single intravenous (iv, 2 mg/kg) and oral (po, 20 mg/kg) administration.

significantly lower than that of control group. Most interestingly, the survival rate of both **8c** treated groups significantly increased when compared with the control group (Figure 8B). Although there is no difference between the 10 and 20 mg/kg of **8c** treated groups in terms of the average tumor size, the 20 mg/kg **8c** treated group showed better survival rate of than 10 mg/kg treated group, as shown in Figure 8B. Together, these preclinical results demonstrated that the potent tumor regression compound **8c** was effective in breast cancer cells both in vitro and in vivo.

Toxicological Evaluation. No significant difference in body weight was observed between mice treated with solvent and **8c** in Figure 9A. Evaluation of numerous histologic sections of these tissues from compound-treated mice did not indicate any detectable pathologic abnormalities, as examined by H&E staining (Figure 9B). In addition, the

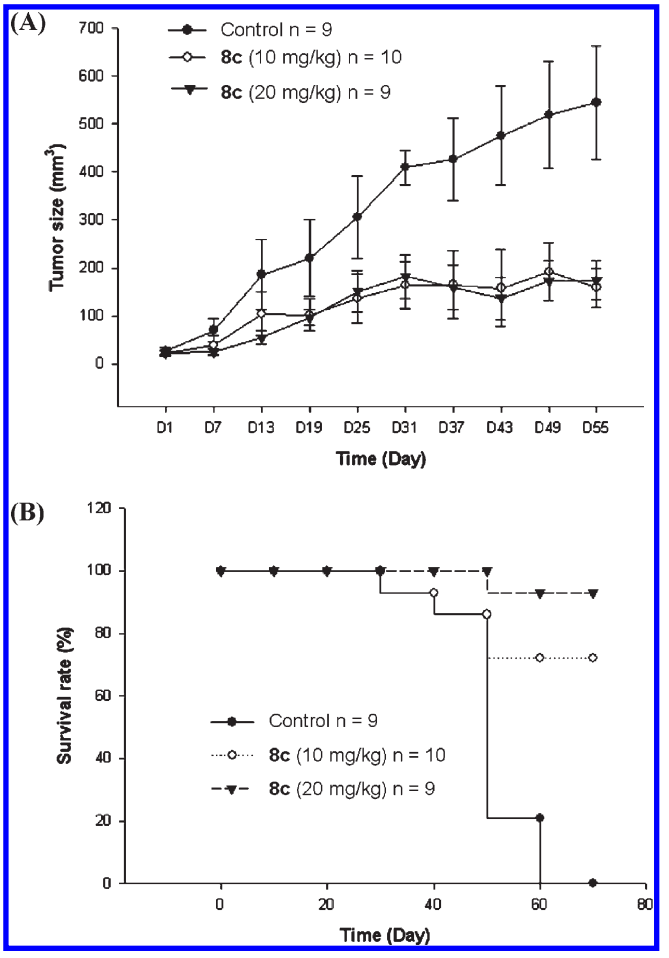

Figure 8. (A) Compound **8c** is a potential compound against breast cancer cell growth in vivo. BT483 cells (2×10^5) were inoculated subcutaneously into the dorsum of nude mice, and intraperitoneal administration (ip) of **8c** was carried out 7 days after the inoculation. The final drug administration concentration was 10 and 20 mg/kg, respectively, and the tumor size was measured at the time indicated. (B) Both 10 and 20 mg/kg **8c** treatments significantly increased the survival rate of the nude mice with BT483-induced breast cancers. Kaplan−Meier survival analysis was used to examine the effect of compound **8c** treatment in a human breast cancer xenograft nude mice model. $P < 0.05$.

compound caused no detectable toxicity on tissues and did not affect organ functions. The organ function tests included liver function tests, such as glutamic oxalacetic transaminase

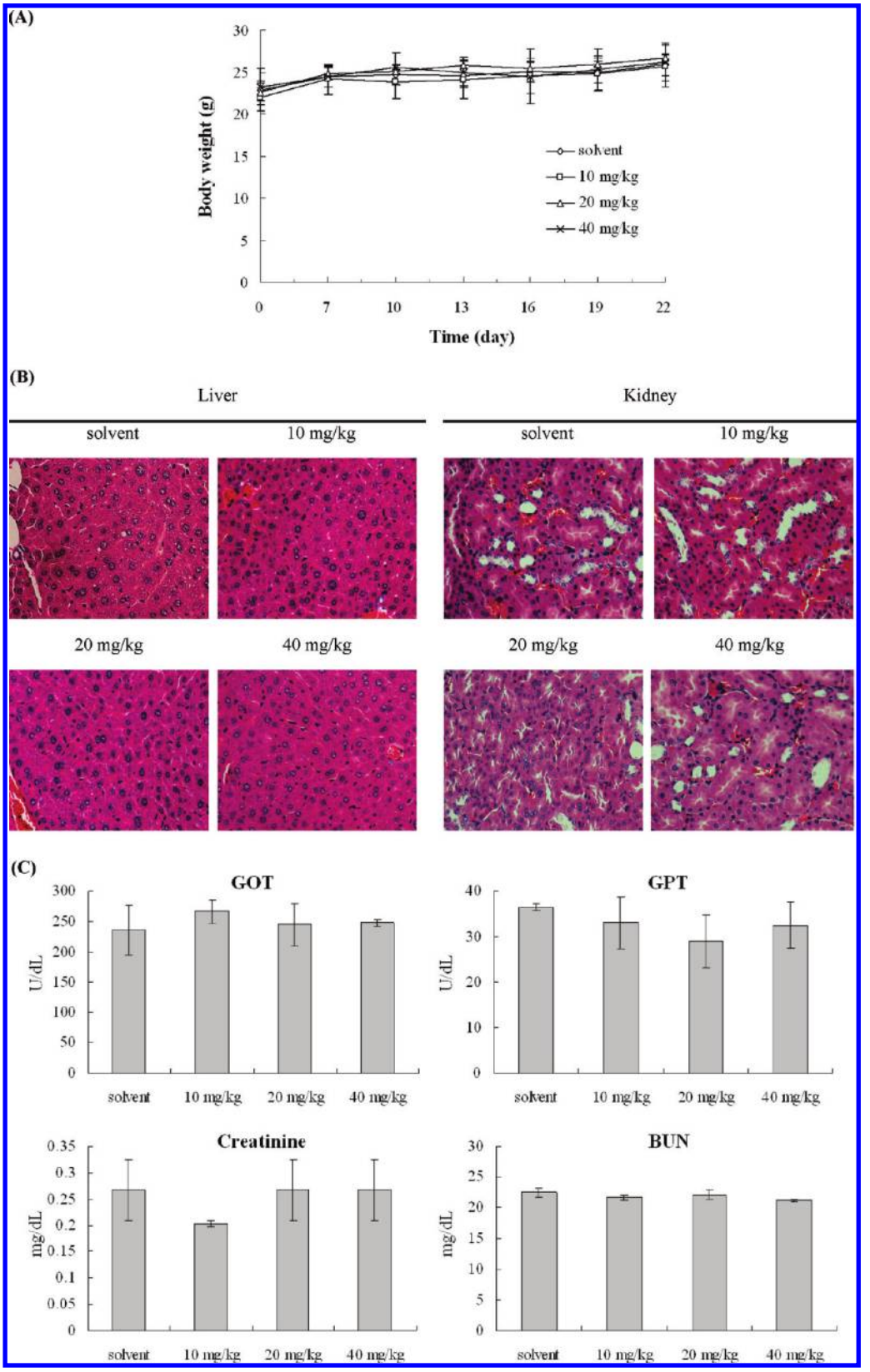

Figure 9. Animals were treated intravenously with **8c** (final dose of 10−40 mg/kg) or solvent control. (A) Effect of compound on body weights in male rats. (B) H&E staining of paraffin-embedded, 5 μm thick sections of the liver and kidney from **8c**-treated and untreated groups of mice observed under 400× magnification. There were no apparent histopathologic differences in these tissues sections. (C) Compound **8c** had no apparent change on serum biochemistry assays of liver and kidney functions. Blood was obtained at the time of sacrifice.

(GOT) and glutamic pyruvic transaminase (GPT), and renal function tests, such as blood urea nitrogen (BUN) and creatinine levels. The organ functions were similar between the **8c** treated and the solvent treated groups (Figure 9C).

Conclusion

We have identified certain indeno[1,2-*c*]quinoline derivatives as a new type of dual topo I and topo II inhibitory agents. Among them, (*E*)-6-hydroxy-9-methoxy-11*H*-indeno[1,2-*c*]-quinolin-11-one *O*-2-(pyrrolidin-1-yl)ethyl oxime (**8c**) was found to be one of the most selective antiproliferative agents with GI_{50} of 0.23, 0.84, 0.89, and 0.79 μM against the growth of HeLa, SAS, A549, and BT483, respectively, and a GI_{50} of 12.44 μM against the growth of skin Detroit-551 normal fibroblast cells. The selective index (SI = (GI_{50} of Detroit-551)/(GI_{50} of HeLa cell)) for **8c** is 54.09, which indicated the high potential for further development. Compound **8c** induced apoptosis through caspase-3 activation, phosphorylation of the histone protein H2AX at Ser139 (γ-H2AX), and DNA fragmentation via cleavage of PARP. Xenographic studies indicated that the tumor mass was effectively reduced by the treatment of tumor-bearing mice at a dose of 20 mg/kg once daily for 14 days.

Experimental Section

General. TLC was done with precoated (0.2 mm) silica gel 60 F_{254} plates from EM Laboratories, Inc. Detection was done by UV light (254 nm). All chromatographic separations were performed using silica gel (Merck 60 230−400 mesh). Melting points were measured with an Electrothermal IA9100 melting point apparatus and were uncorrected. ^{1}H and ^{13}C NMR spectra were obtained with a Varian-Unity-400 spectrometer at 400 and 100 MHz. Chemical shifts δ in ppm were measured with $SiMe_4$ as an internal standard (=0 ppm). Coupling constants *J* are reported in Hz. Elemental analyses were carried out on a Heraeus CHN-O rapid elemental analyzer, and results were within ±0.4% of calculated values. The purity of all target compounds used in the biophysical and biological studies was ≥95%.

9-Methoxy-11*H*-indeno[1,2-*c*]quinolin-11-one (3). To a stirred solution of sodium (0.1 g) in dry EtOH (40 mL) was added a solution of 6-chloro-9-methoxy-11*H*-indeno[1,2-*c*]quinolin-11-one (**2**, 0.30 g, 1.0 mmol) in EtOH (10 mL). The mixture was refluxed for 48 h (TLC monitoring), and solvent was evaporated. The crude product was purified by flash column chromatography (FC, silica gel, using CH_2Cl_2/MeOH = 50:1 as the eluent) to give **3** (0.15 g, 58%) as a red solid. Mp: 195−196 °C. ^{1}H NMR (400 MHz, $CDCl_3$): 3.87 (s, 3H, 9-OMe), 6.94 (dd, 1H, *J* = 8.0, 2.4 Hz, 8-H), 7.20 (d, 1H, *J* = 2.4 Hz, 10-H), 7.47 (d, 1H, *J* = 8.0 Hz, 7-H), 7.57−7.66 (m, 2H, 2- and 3-H), 8.02−8.04 (m, 1H, 4-H), 8.71−8.73 (m, 1H, 1-H), 9.11 (s, 1H, 6-H). ^{13}C NMR (100 MHz, $CDCl_3$): 55.83, 111.14, 119.56, 121.77, 123.44, 123.91, 129.47, 129.65, 129.82, 133.03, 134.83, 135.37, 138.23, 143.11, 149.73, 161.44, 194.99. Anal. Calcd for $C_{17}H_{11}NO_2$: C 78.15, H 4.24, N 5.36. Found: C 77.95, H 4.25, N 5.35.

(*E*)-9-Methoxy-11*H*-indeno[1,2-*c*]quinolin-11-one Oxime (4). To a suspension of **3** (0.26 g, 1.0 mmol) in 2-ethoxyethanol (30 mL) was added hydroxylamine·HCl (0.20 g, 3.0 mmol). The reaction mixture was heated with stirring under microwave irradiation (100 W) for 30 min (TLC monitoring). The solvent was removed in vacuo, and the residue was poured into H_2O (20 mL). The resulting precipitate was recrystallized from MeOH to give **4** (0.24 g, 85%) as a red solid. Mp: 270−271 °C. ^{1}H NMR (400 MHz, DMSO-d_6): 3.84 (s, 3H, OCH_3), 7.13 (dd, 1H, *J* = 8.4, 2.8 Hz, 8-H), 7.82−7.96 (m, 3H, 2-, 3-, and 10-H), 8.05 (d, 1H, *J* = 8.4 Hz, 7-H), 8.27−8.29 (m, 1H, 4-H), 8.84−8.86 (m, 1H, 1-H), 9.68 (s, 1H, 6-H), 14.24 (s, 1H, NOH). ^{13}C NMR (100 MHz, DMSO-d_6): 55.65, 114.35, 116.54, 122.73, 123.36, 123.83, 125.69, 128.68, 130.09, 130.51, 131.75, 133.49, 139.04, 140.19, 141.42, 152.90, 160.97. Anal. Calcd for $C_{17}H_{12}N_2O_2 \cdot 0.9H_2O \cdot 0.7HCl$: C 64.19, H 4.38, N 8.81. Found: C 63.91, H 4.38, N 8.81.

(*E*)-9-Methoxy-11*H*-indeno[1,2-*c*]quinolin-11-one *O*-2-(dimethylamino)ethyl Oxime (5a). To a stirred solution of **4** (0.28 g, 1 mmol) in dry DMF (20 mL) was added NaH (60% in oil, 0.50 g) at 0 °C, and stirring was continued for 1 h. After the mixture was stirred at room temperature for 8 h, 2-chloro-*N*,*N*-dimethylethanamine, HCl (0.42 g, 3 mmol) was added, and stirring was continued for 1 h (TLC monitoring). The reaction mixture was partitioned between H_2O (50 mL) and CH_2Cl_2 (50 mL). The organic layer was collected, dried over $MgSO_4$, and evaporated in vacuo to give the residue which was purified by FC (using CH_2Cl_2/MeOH = 10:1) to give **5a** (0.20 g, 56%). Mp: 116−117 °C. ^{1}H NMR (400 MHz, $CDCl_3$): 2.42 (s, 6H, NMe_2), 2.93 (t, 2H, *J* = 6.0 Hz, OCH_2CH_2N), 3.89 (s, 3H, 9-OMe), 4.72 (t, 2H, *J* = 6.0 Hz, OCH_2CH_2N), 6.97 (dd, 1H, *J* = 8.4, 2.4 Hz, 8-H), 7.55−7.67 (m, 3H, 2-, 3-, and 7-H), 7.95 (d, 1H, *J* = 2.4 Hz, 10-H), 8.07−8.10 (m, 1H, 4-H), 8.82−8.84 (m, 1H, 1-H), 9.16 (s, 1H, 6-H). ^{13}C NMR (100 MHz, $CDCl_3$): 45.94 (2C), 55.67, 58.13, 74.94, 115.90, 116.19, 120.64, 123.94, 125.66, 128.17, 128.56, 130.15, 131.53, 131.88, 133.66, 136.47, 142.94, 148.21, 154.45, 160.53. Anal. Calcd for $C_{21}H_{21}N_3O_2$: C 72.60, H 6.09, N 12.10. Found: C 72.47, H 6.11, N 12.01.

(*E*)-9-Methoxy-11*H*-indeno[1,2-*c*]quinolin-11-one *O*-3-(dimethylamino)propyl Oxime (5b). 5b was obtained from **4** and 3-chloro-*N*,*N*-dimethylpropanamine·HCl as described for **5a**: 48% yield. Mp: 80−81 °C. ^{1}H NMR (400 MHz, $CDCl_3$): 2.09−2.18 (m, 2H, $OCH_2CH_2CH_2N$), 2.30 (s, 6H, NMe_2), 2.55 (t, 2H, *J* = 7.2 Hz, $OCH_2CH_2CH_2N$), 3.87 (s, 3H, 9-OMe), 4.60 (t, 2H, *J* = 6.4 Hz, $OCH_2CH_2CH_2N$), 6.93 (dd, 1H, *J* = 8.4, 2.4 Hz, 8-H), 7.53−7.64 (m, 3H, 2-, 3-, and 7-H), 7.87 (d, 1H, *J* = 2.4 Hz, 10-H), 8.06−8.08 (m, 1H, 4-H), 8.80−8.82 (m, 1H, 1-H), 9.13 (s, 1H, 6-H). ^{13}C NMR (100 MHz, $CDCl_3$): 27.53, 45.45 (2C), 55.62, 56.31, 75.05, 115.59, 116.08, 120.56, 123.90, 125.69, 128.07, 128.51, 130.05, 131.46, 131.79, 133.52, 136.49, 142.87, 148.12, 154.03, 160.44. Anal. Calcd for $C_{22}H_{23}N_3O_2 \cdot 1.25H_2O$: C 68.81, H 6.71, N 10.95. Found: C 68.78, H 6.68, N 10.87.

(*E*)-9-Methoxy-11*H*-indeno[1,2-*c*]quinolin-11-one *O*-2-(pyrrolidin-1-yl)ethyl Oxime (5c). 5c was obtained from **4** and 1-(2-chloroethyl)pyrrolidine·HCl as described for **5a**: 56% yield. Mp: 85−86 °C. ^{1}H NMR (400 MHz, $CDCl_3$): 1.78−1.85 (m, 4H, pyrroidinyl-H), 2.67−2.72 (m, 4H, pyrroidinyl-H), 3.05 (t, 2H, *J* = 6.0 Hz, OCH_2CH_2N), 3.86 (s, 3H, 9-OMe), 4.71 (t, 2H, *J* = 6.0 Hz, OCH_2CH_2N), 6.94 (dd, 1H, *J* = 8.4, 2.4 Hz, 8-H), 7.53−7.64 (m, 3H, 2-, 3-, and 7-H), 7.91 (d, 1H, *J* = 2.4 Hz, 10-H), 8.06−8.08 (m, 1H, 4-H), 8.79−8.82 (m, 1H, 1-H), 9.12 (s, 1H, 6-H). ^{13}C NMR (100 MHz, $CDCl_3$): 23.52 (2C), 54.81 (2C), 54.89, 55.62, 76.05, 115.84, 116.00, 120.56, 123.89, 125.67, 128.10, 128.51, 130.06, 131.45, 131.80, 133.55, 136.45, 142.86, 148.13, 154.20, 160.44. Anal. Calcd for $C_{23}H_{23}N_3O_2 \cdot 0.5EtOH \cdot 0.1HCl$: C 72.03, H 6.59, N 10.50. Found: C 72.05, H 6.33, N 10.30.

(*E*)-9-Methoxy-11*H*-indeno[1,2-*c*]quinolin-11-one *O*-2-(piperdin-1-yl)ethyl Oxime (5d). 5d was obtained from **4** and 1-(2-chloroethyl)piperidine·HCl as described for **5a**: 71% yield. Mp: 101−102 °C. ^{1}H NMR (400 MHz, $CDCl_3$): 1.43−1.49 (m, 2H, piperidinyl-H), 1.61−1.66 (m, 4H, piperidinyl-H), 2.56−2.58 (m, 4H, piperidinyl-H), 2.93 (t, 2H, *J* = 6.0 Hz, OCH_2CH_2N), 3.88 (s, 3H, 9-OMe), 4.72 (t, 2H, *J* = 6.0 Hz, OCH_2CH_2N), 6.95 (dd, 1H, *J* = 8.0, 2.4 Hz, 8-H), 7.54−7.65 (m, 3H, 2-, 3-, and 7-H), 7.92 (d, 1H, *J* = 2.4 Hz, 10-H), 8.06−8.09 (m, 1H, 4-H), 8.80−8.83 (m, 1H, 1-H), 9.14 (s, 1H, 6-H). ^{13}C NMR (100 MHz, $CDCl_3$): 24.14, 25.97 (2C), 55.03 (2C), 55.67, 57.92, 74.93, 115.91, 116.02, 120.59, 123.92, 125.71, 128.12, 128.53, 130.11, 131.51, 131.86, 133.58, 136.50, 142.90, 148.19, 154.21, 160.50. Anal. Calcd for $C_{28}H_{32}N_4O_4 \cdot 0.2H_2O$: C 73.70, H 6.56, N 10.75. Found: C 73.88, H 6.53, N 10.77.

(*E*)-9-Methoxy-11*H*-indeno[1,2-*c*]quinolin-11-one *O*-2-morpholinoethyl Oxime (5e). 5e was obtained from **4** and 1-(2-chloroethyl)morpholine·HCl as described for **5a**: 69% yield. Mp: 110−112 °C. ^{1}H NMR (400 MHz, $CDCl_3$): 2.63−2.65 (m, 4H, mopholinyl-H), 2.96 (t, 2H, *J* = 6.0 Hz, OCH_2CH_2N), 3.74−3.77 (m, 4H, mopholinyl-H), 3.88 (s, 3H, 9-OMe), 4.72 (t, 2H,

J = 6.0 Hz, OC$\underline{H_2}$CH$_2$N), 6.95 (dd, 1H, J = 8.4, 2.4 Hz, 8-H), 7.54−7.65 (m, 3H, 2-, 3-, and 7-H), 7.92 (d, 1H, J = 2.4 Hz, 10-H), 8.07−8.09 (m, 1H, 4-H), 8.79−8.82 (m, 1H, 1-H), 9.15 (s, 1H, 6-H). ^{13}C NMR (100 MHz, $CDCl_3$): 54.02 (2C), 55.68, 57.58, 66.92 (2C), 74.36, 115.61, 116.40, 120.64, 123.90, 125.61, 128.14, 128.56, 130.16, 131.49, 131.87, 133.64, 136.41, 142.93, 148.201, 154.42, 160.52. Anal. Calcd for $C_{23}H_{23}N_3O_3 \cdot 0.2H_2O$: C 70.27, H 6.01, N 10.69. Found: C 70.01, H 5.91, N 10.59.

6-Hydroxy-9-methoxy-11*H*-indeno[1,2-*c*]quinolin-11-one (6). A mixture of **2** (0.30 g, 1.0 mmol) and 36% HCl (2 mL) in DMF (30 mL) was refluxed for 2 h (TLC monitoring). The mixture was evaporated in vacuo, treated with H_2O (20 mL), and filtered and the crude solid was recrystallized from MeOH to give **6** (0.09 g, 32%) as a red solid. Mp: 316−317 °C. ^{1}H NMR (400 MHz, DMSO-d_6): 3.83 (s, 3H, 9-OMe), 7.05 (dd, 1H, J = 8.0, 2.4 Hz, 8-H), 7.14 (d, 1H, J = 2.4 Hz, 10-H), 7.24−7.28 (m, 1H, 2-H), 7.37 (d, 1H, J = 8.4 Hz, 4-H), 7.49−7.53 (m, 1H, 3-H), 7.81 (d, 1H, J = 8.0 Hz, 7-H), 8.34 (d, 1H, J = 8.4 Hz, 1-H), 12.32 (s, 1H, NH). ^{13}C NMR (100 MHz, DMSO-d_6): 55.72, 111.14, 114.79, 115.64, 118.17, 123.10, 123.40, 124.37, 130.16, 133.13, 133.37, 133.90, 137.78, 139.76, 158.71, 160.55, 195.10. HRMS (ESI) calcd for $C_{17}H_{12}NO_3$ (M^+) 278.0817; found 278.0818.

(*E*)-6-hydroxy-9-methoxy-11*H*-indeno[1,2-*c*]quinolin-11-one Oxime (7). 7 was obtained from **6** as described for **4**: 85% yield. Mp: 320−321 °C. ^{1}H NMR (400 MHz, DMSO-d_6): 3.82 (s, 3H, OCH_3), 7.03 (dd, 1H, J = 2.4, 8.4 Hz), 7.21−7.25 (m, 1H), 7.39−7.41 (m, 1H), 7.45−7.50 (m, 1H), 7.89 (d, 1H, J = 2.4 Hz), 8.03 (d, 1H, J = 8.4 Hz), 8.56 (dd, 1H, J = 1.6, 8.4 Hz), 12.00 (s, 1H, OH), 13.62 (1H, NOH). ^{13}C NMR (100 MHz, DMSO-d_6): 55.54, 114.95, 115.04, 115.91, 115.93, 122.50, 123.37, 125.44, 129.40, 129.45, 129.94, 131.02, 137.91, 138.82, 154.07, 158.79, 195.76. Anal. Calcd for $C_{17}H_{12}N_2O_3 \cdot 0.2H_2O$: C 69.00, H 4.23, N 9.47. Found: C 69.03, H 4.41, N 9.09.

(*E*)-6-Hydroxy-9-methoxy-11*H*-indeno[1,2-*c*]quinolin-11-one *O*-2-(Dimethylamino)ethyl Oxime (8a). To a suspension of **6** (0.28 g, 1.0 mmol) in 2-ethoxyethanol (30 mL) was added 2-(*N*,*N*-dimethylamino)ethoxyamine·HCl[61] (0.42 g, 3.0 mmol). The reaction mixture was refluxed for 2 h (TLC monitoring). The solvent was removed in vacuo and the residue suspended in H_2O (20 mL). The crude product was collected and purified by FC (using CH_2Cl_2/MeOH = 10:1) to give **8a** (0.29 g, 81%) as a red solid. Mp: 262−263 °C (dec). ^{1}H NMR (400 MHz, $CDCl_3$): 2.41 (s, 6H, NMe_2), 2.90 (t, 2H, J = 6.0 Hz, OCH$_2$C$\underline{H_2}$N), 3.85 (s, 3H, 9-OMe), 4.68 (t, 2H, J = 6.0 Hz, OC$\underline{H_2}$CH$_2$N), 6.90 (dd, 1H, J = 8.4, 2.4 Hz, 8-H), 7.15−7.19 (m, 1H, 2-H), 7.35−7.41 (m, 2H, 3- and 4-H), 7.80 (d, 1H, J = 2.4 Hz, 10-H), 8.11 (d, 1H, J = 8.4 Hz, 7-H), 8.57 (d, 1H, J = 8.0 Hz, 1-H), 12.11 (br s, 1H, 6-OH). ^{13}C NMR (100 MHz, $CDCl_3$): 45.99 (2C), 55.56, 58.22, 75.14, 115.08, 115.70, 116.23, 116.93, 123.03, 123.94, 126.10, 129.24, 129.95, 130.84, 131.93, 138.42, 138.99, 154.68, 160.00, 160.62. Anal. Calcd for $C_{21}H_{21}N_3O_3 \cdot 0.6H_2O$: C 67.39, H 5.99, N 11.23. Found: C 67.23, H 5.72, N 11.17.

(*E*)-6-Hydroxy-9-methoxy-11*H*-indeno[1,2-*c*]quinolin-11-one *O*-3-(Dimethylamino)propyl Oxime (8b). 8b was obtained from **6** and 3-(*N*,*N*-dimethylamino)propoxyamine·HCl[61] as described for **8a**: 75% yield. Mp: 185−186 °C. ^{1}H NMR (400 MHz, $CDCl_3$): 2.14 (quin, 2H, J = 6.4 Hz, OCH$_2$C$\underline{H_2}$CH$_2$N), 2.33 (s, 6H, NMe_2), 2.58 (t, 2H, J = 7.8 Hz, OCH$_2$C$\underline{H_2}$C$\underline{H_2}$N), 3.88 (s, 3H, 9-OMe), 4.62 (t, 2H, J = 6.4 Hz, OC$\underline{H_2}$CH$_2$C$\underline{H_2}$N), 6.94 (dd, 1H, J = 8.4, 2.4 Hz, 8-H), 7.16−7.20 (m, 1H, 2-H), 7.33 (d, 1H, J = 7.2 Hz, 4-H), 7.38−7.43 (m, 1H, 3-H), 7.81 (d, 1H, J = 2.4 Hz, 10-H), 8.15 (d, 1H, J = 8.0 Hz, 7-H), 8.60−8.62 (m, 1H, 1-H), 11.38 (br s, 1H, 6-OH). ^{13}C NMR (100 MHz, $CDCl_3$): 27.54, 45.42 (2C), 55.65, 56.78, 75.13, 114.92, 115.81, 115.97, 116.94, 123.13, 123.99, 126.23, 129.36, 129.97, 130.84, 131.88, 138.26, 139.06, 154.46, 160.10, 160.32. ESIMS [M + H]$^+$: 378.

(*E*)-6-Hydroxy-9-methoxy-11*H*-indeno[1,2-*c*]quinolin-11-one *O*-2-(pyrrolidin-1-yl)ethyl Oxime (8c). 8c was obtained from **6** and 2-(pyrrolidin-1-yl)ethoxyamine·HCl[61] as described for **8a**: 82% yield. Mp: 240−242 °C (dec). ^{1}H NMR (400 MHz, $CDCl_3$): 1.80−1.87 (m, 4H, pyrroidinyl-H), 2.70−2.73 (m, 4H, pyrroidinyl-H), 3.07 (t, 2H, J = 6.0 Hz, OCH$_2$C$\underline{H_2}$N), 3.85 (s, 3H, 9-OMe), 4.72 (t, 2H, J = 6.0 Hz, OC$\underline{H_2}$CH$_2$N), 6.88 (dd, 1H, J = 8.4, 2.4 Hz, 8-H), 7.14−7.18 (m, 1H, 2-H), 7.33−7.40 (m, 2H, 3- and 4-H), 7.78 (d, 1H, J = 2.4 Hz, 10-H), 8.09 (d, 1H, J = 8.0 Hz, 7-H), 8.56 (d, 1H, J = 8.0 Hz, 1-H), 12.11 (br s, 1H, 6-OH). ^{13}C NMR (100 MHz, $CDCl_3$): 23.54 (2C), 54.78 (2C), 54.93, 55.59, 76.05, 115.08, 115.65, 116.19, 116.91, 123.05, 123.93, 126.13, 129.24, 129.92, 130.80, 131.93, 138.39, 138.98, 154.62, 159.99, 160.55. Anal. Calcd for $C_{23}H_{23}N_3O_2 \cdot 1.5HCl$: C 62.18, H 5.57, N 9.46. Found: C 62.01, H 5.93, N 9.36.

(*E*)-6-Hydroxy-9-methoxy-11*H*-indeno[1,2-*c*]quinolin-11-one *O*-2-(Piperidin-1-yl)ethyl Oxime (8d). 8d was obtained from **6** and 2-(piperidin-1-yl)ethoxyamine·HCl[61] as described for **8a**: 84% yield. Mp: 241−242 °C (dec). ^{1}H NMR (400 MHz, DMSO-d_6): 1.36−1.40 (m, 2H, piperidinyl-H), 1.48−1.54 (m, 4H, piperidinyl-H), 2.51−2.53 (m, 4H, piperidinyl-H), 2.81 (t, 2H, J = 5.2 Hz, OCH$_2$C$\underline{H_2}$N), 3.83 (s, 3H, 9-OMe), 4.67 (t, 2H, J = 5.2 Hz, OC$\underline{H_2}$CH$_2$N), 7.06 (dd, 1H, J = 8.4, 2.4 Hz, 8-H), 7.22−7.26 (m, 1H, 2-H), 7.39−7.41 (m, 1H, 4-H), 7.47−7.51 (m, 1H, 3-H), 7.82 (d, 1H, J = 2.4 Hz, 10-H), 8.02 (d, 1H, J = 8.4 Hz, 7-H), 8.53−8.55 (m, 1H, 1-H), 12.06 (br s, 1H, 6-OH). ^{13}C NMR (100 MHz, DMSO-d_6): 23.89, 25.59 (2C), 54.28 (2C), 55.54, 57.36, 74.61, 115.46 (2C), 115.66, 115.92, 122.67, 123.59, 125.38, 129.24, 129.61, 130.55, 131.32, 137.19, 138.85, 153.91, 158.59, 159.83. Anal. Calcd for $C_{24}H_{25}N_3O_3 \cdot 0.1H_2O$: C 71.11, H 6.28, N 10.37. Found: C 70.95, H 6.12, N 10.31.

(*E*)-6-Hydroxy-9-methoxy-11*H*-indeno[1,2-*c*]quinolin-11-one *O*-2-Morpholinoethyl Oxime (8e). 8e was obtained from **6** and 2-morpholinoethoxyamine·HCl[61] as described for **8a**: 85% yield. Mp: 255−256 °C. ^{1}H NMR (400 MHz, $CDCl_3$): 2.64−2.66 (m, 4H, morpholinyl-H), 2.95 (t, 2H, J = 5.6 Hz, OCH$_2$-C$\underline{H_2}$N), 3.75−3.77 (m, 4H, morpholinyl-H), 3.86 (s, 3H, 9-OMe), 4.70 (t, 2H, J = 5.6 Hz, OC$\underline{H_2}$CH$_2$N), 6.92 (dd, 1H, J = 8.4, 2.4 Hz, 8-H), 7.17−7.21 (m, 1H, 2-H), 7.38−7.45 (m, 2H, 3- and 4-H), 7.80 (d, 1H, J = 2.4 Hz, 10-H), 8.13 (d, 1H, J = 8.4 Hz, 7-H), 8.57−8.59 (m, 1H, 1-H), 12.09 (br s, 1H, 6-OH). ^{13}C NMR (100 MHz, $CDCl_3$): 54.04 (2C), 55.62, 57.60, 66.94 (2C), 74.73, 114.92, 115.96, 116.27, 116.92, 123.10, 124.01, 126.07, 129.36, 129.93, 130.90, 131.91, 138.41, 139.01, 154.76, 160.06, 160.63. Anal. Calcd for $C_{23}H_{23}N_3O4 \cdot 0.3H_2O$: C 67.23, H 5.80, N 10.23. Found: C 67.11, H 5.53, N 10.16.

(*E*)-9-Methoxy-6-(piperazin-1-yl)-11*H*-indeno[1,2-*c*]quinolin-11-one *O*-2-(Pyrrolidin-1-yl)ethyl Oxime (10c). 10c was obtained from **9** and 1-(2-chloroethyl)pyrrolidine·HCl as described for **5a**: 43% yield. Mp: 126−128 °C. ^{1}H NMR (400 MHz, DMSO-d_6): 1.67−1.71 (m, 4H, pyrrolidinyl-H), 2.53−2.57 (m, 4H, pyrrolidinyl-H), 2.94 (t, 2H, J = 5.6 Hz, OCH$_2$C$\underline{H_2}$N), 2.93−2.97 (m, 4H, piperazinyl-H), 3.19−3.23 (m, 4H, piperazinyl-H), 3.83 (s, 3H, 9-OMe), 4.64 (t, 2H, J = 5.6 Hz, OC$\underline{H_2}$CH$_2$N), 7.13 (dd, 1H, J = 8.4, 2.4 Hz, 8-H), 7.46−7.48 (m, 1H, 2-H), 7.59−7.60 (m, 1H, 3-H), 7.75 (d, 1H, J = 8.4 Hz, 7-H), 7.80 (d, 1H, J = 8.4 Hz, 4-H), 7.89 (d, 1H, J = 2.4 Hz, 10-H), 8.70 (dd, 1H, J = 8.4, 1.2 Hz, 1-H). ^{13}C NMR (100 MHz, DMSO-d_6): 23.22 (2C), 45.08 (2C), 50.37 (2C), 54.08 (2C), 54.38, 55.50, 75.82, 115.48, 115.82, 120.85, 123.78, 124.97, 125.93, 126.87, 128.17, 128.90, 130.35, 131.01, 138.05, 146.54, 153.60, 156.95, 159.62. Anal. Calcd for $C_{27}H_{31}N_5O_2 \cdot 0.4H_2O$: C 69.78, H 6.90, N 15.07. Found: C 69.75, H 6.90, N 14.69.

Cell Lines and Culture Conditions. Cancer cells were purchased from Bioresource Collection and Research Center (Hsinchu, Taiwan). Each cell line was maintained in standard medium and grown as a monolayer in Dulbecco's modified Eagle's medium (DMEM) containing 10% fetal bovine serum, 2 mM glutamine, 100 units/mL penicillin, and 100 g/mL streptomycin. Cultures were maintained at 37 °C with 5% CO_2 in a humidified atmosphere.

Cell Proliferation and Cell Viability MTT Assay.[62] The 3-[4,5-dimethylthiazol-2-yl]-2,5-diphenyltetrazolium bromide (MTT, 2 mg/mL) dye reduction assay was used. Cells were plated in 96-well microtiter plates at a density of 5×10^3/well and incubated for 24 h. After that, they were treated with vehicle alone (controls) or compounds (drugs dissolved in DMSO) at the concentrations indicated. Treated cells were incubated for an additional 48 h. Cell survival is expressed as a percentage of control-cell growth. The assay spectrophotometrically measures the reduction of MTT by mitochondrial dehydrogenases of viable cells to a blue formazan product. Tumor cells were incubated in each well with serial dilutions of the tested compounds. After they had been incubated (37 °C, 5% CO_2 in a humid atmosphere) for 2 days, 100 μL of MTT (2 mg/mL in PBS) was added to each well and the plate was incubated for an additional 2 h. The resulting formazan was dissolved in 100 μL of DMSO and read at 570 nm. The percentage of growth inhibition was calculated by using the following equation: percentage growth inhibition = $(1 - A_t/A_c) \times 100$, where A_t and A_c are the absorbance in treated and control cultures, respectively. The drug concentration causing a 50% cell growth inhibition (GI_{50}) was determined by interpolation from dose-response curves. All experiments were done three times.

Topoisomerases (topo I and topo II) Inhibition Assay.[63,64] Type I or type II DNA topoisomerase was assayed by measuring the decreased mobility of the relaxed isomers of supercoiled pBR322 DNA in an agarose gel after it had been treated with human topo I or II. The standard topoisomerase assay mixture (20 μL) contained 40 mM Tris-HCl (pH 7.5), 100 mM KCl, 10 mM DTT, 0.5 mM EDTA, 10 mM $MgCl_2$, 30 μg/mL BSA, 0.2 μg of pBR322 DNA, and 2 units of enzyme (1 unit is defined as the amount of enzyme required to convert 0.2 μg of supercoiled DNA substrate to the relaxed form under standard assay conditions). Reactions were done at 37 °C for 30 min and then terminated by adding 0.5% SDS, 0.25 μg/mL bromophenol blue, and 15% glycerol. The samples were electrophoresed in a horizontal 1% agarose gel in Tris-acetate/EDTA buffer (40 mM Tris-acetate, 2 mM EDTA [pH 8]) at 1.5 V/cm for 2−3 h at room temperature. DMSO concentrations in each reaction were maintained at 1% by adding serially diluted drug stocks so as not to produce solvent-mediated inhibition of topo I or II activity. The gels were stained with ethidium bromide (5 μg/mL), destained in water, and photographed under UV light. The relaxation percentage was measured using a laser microdensitometer (2202 Ultrascan, LKB, Bromma, Stockholm, Sweden) to analyze negative photographs of supercoiled monomer DNA band fluorescence after ethidium bromide staining, and the area under the peak was calculated.

Flow Cytometry Analysis.[64] Apoptosis and cell cycle profiles were assessed using DNA fluorescence flow cytometry. HeLa cells treated with DMSO or **8c** at 0.1, 0.3, or 1 μM for 24 h were harvested, rinsed in PBS, resuspended, and fixed in 80% ethanol and then stored at −20 °C in fixation buffer until they were ready for analysis. The pellets were suspended in 1 mL of fluorochromic solution (0.08 mg/mL PI), 0.1% Triton X-100, and 0.2 mg/mL RNase A in 1× PBS) at room temperature in the dark for 30 min. The DNA content was analyzed using a flow cytometer (FACScan, Becton Dickinson, Mountain View, CA) and CellQuest software (Becton Dickinson). The population of apoptotic nuclei (subdiploid DNA peak in the DNA fluorescence histogram) is expressed as a percentage of the entire population.

Immunofluorescence Analysis.[65,66] Cells were seeded (1×10^4/well) into a 12-well plate until 50−60% confluent and treated for 24 h with 0.3 and 1 μM **8c**. After they had been incubated, the cells were washed twice with warm PBS and fixed in 4% paraformaldehyde for 1 h. They were then washed for 5 min with PBS that contained 0.1 M glycine and permeabilized with solution containing 2% FBS and 0.4% Triton X-100 in PBS at room temperature for 15 min. After they had been permeabilized, the cells were stained with 0.1 μg/mL of 4′-6-diamidino-2-phenylindole (DAPI) in PBS for 10 min in the dark. The excess DAPI solution was then removed, and the cells were washed twice with PBS. The samples were mounted and analyzed under the fluorescence microscope's CCD camera.

Protein Extraction and Immunoblotting.[65,66] After the cells had been treated with vehicle (1% DMSO) or tested compounds at various concentrations for 48 h, the cells were washed twice with PBS and the reaction was terminated by adding 100 μL of lysis buffer. For Western blot analysis, the 50 μg of protein was separated using electrophoresis in 15% SDS−PAGE and transferred to a nitrocellulose membrane. After it had been incubated overnight at 4 °C in TBST/5% nonfat milk, the membrane was washed three times with TBST and then immunoreacted with monoclonal primary antibodies for 2 h at room temperature on a shaker. Appropriate antibodies to anti-caspase-3, anti-poly-ADP-ribose polymerase (PARP), anti-γ-H2Ax, and anti-β-actin (Cell Signaling Technology) were used. After the membrane had been washed four more times with TBST, anti-mouse or anti-rabbit IgG (dilution 1:10000) was applied to the membranes for 1 h at room temperature. The membranes were then washed with TBST for 1 h, and the signals were detected using enhanced chemiluminescence (ECL) reagents.

Human Breast Cancer Xenograft Nude Mice Model. Human breast cancer tumor xenograft assay was adapted from previously published methods.[67] Balb/C athymic nude mice, age 6−8 weeks, weighing around 20 g were used and maintained in sterile isolators at the small animal facility in NCKU. Briefly, human breast tumor xenografts were established in nude mice by subcutaneous inoculation of a single cell suspension of BT483 cells (0.5×10^6 cells/100 μL). The tumor bearing animals were divided into two groups of three animals each (**8c**, 10 and 20 mg/kg treatments and control). Treatment with **8c** was initiated when the average tumor volumes, as measured using a vernier caliper, were around 500 mm^3. The test compound was formulated using a cosolvent formulation, diluted in 5% dextrose, and administered intravenously to the treatment group of tumor-bearing animals at a dose of 10 or 20 mg/kg once daily for 14 days. Control animals received an equivalent volume of vehicle alone for the same period. After daily drug administration, tumor size was measured by using a caliper and the tumor volumes were calculated as (width) × (length) × (height). Kaplan−Meier survival analysis was then used to examine the survival effect of **8c** treatment in the end of experiment. A value of $p < 0.05$ was considered significant.

Statistical Analysis. Data are presented as the mean ± SEM (standard error of the mean) from at least three separate experiments. Statistical analyses used the Bonferroni *t*-test after ANOVA for multigroup comparison and Student's *t*-test for two-group comparison. $P < 0.05$ was considered significant. Linear regression analysis (at least three data points within 20−80% inhibition) was used to calculate GI_{50} values. The software used for these analyses was Prism 4.0 (GraphPad Software Inc., San Diego, CA).

QSAR Modeling.[68] We employed a support vector machine (LibSVM implementation in Weka, ε-SVR variety, radial basis function kernel) algorithm to train a regression model that predicts GI_{50} values from the molecular descriptors of the experimentally analyzed compounds and used 100 runs of 4-fold cross validation in the Weka experimenter to test its predictive strength. A Pearson's correlation coefficient r was computed between the predicted and the actual $\log GI_{50}$ values in each testing fold, and the average of 400 such correlation coefficients (4×100 runs) is reported as the estimated model performance on unseen data. Prior to training, we have applied principal component analysis (PCA) to the data to reduce the number of attributes and filter out noise; normalization in Weka's PCA was turned off, as the attributes were already standardized. Retaining 95% of the original descriptor information generated 9 principal components or 10 if the 7 molecules from Leevy et al.

were included. Using Weka Experimenter, we simultaneously optimized (i) the SVM parameter c (controls complexity and generalization properties of models), (ii) the SVM parameter γ (controls the shape of the regression hyperplane), and (iii) the number of principal components discarded to maximize the model performance estimate (r, above). Normalization option of the LibSVM in Weka was switched on; all the other parameters were left at default values. Parameters c and γ were varied exponentially, from 10^{-2} to 10^{3} (c) and from 10^{-3} to 10^{2} (γ) in increments of 101; after selection of the optimal number of PCs, c and γ, a second iteration of "fine-tuning" of c and γ was used where the two parameters were varied exponentially from $10^{\text{OptimalValue}} - 1$ to $10^{\text{OptimalValue}+1}$ in increments of $10^{0.1}$. For the original 16-molecule data set, the highest performance was achieved for two principal components (PCs) at $r = 0.739$, $c = 10^{1.1}$, and $r = 10^{1.1}$. For the refined 15-molecule data set, the highest "peak" in performance was observed at 5 PCs ($r = 0.785$); however, a close second ($r = 0.772$) was observed with only two PCs at $c = 10^{0.2}$ and $r = 10^{0.4}$. We decided in favor of the latter model because a much simpler representation of the descriptor space with a similar performance is less likely to overfit and therefore more desirable. When molecules from Leevy et al.[69] were added (15 + 7 = 22 molecules), optimal performance ($r = 0.802$, cross-validation on 15 training set molecules) was achieved for three PCs at $c = 10^{0.5}$ and $r = 10^{0.1}$. The trained SVM model was then used to predict GI_{50} values for the seven compounds from Leevy et al. The errors in the predicted activity of the individual molecules were measured by computing the absolute difference between the rank of the predicted log GI_{50} among all of the predictions using leave-one-out cross-validation and the rank of the actual log GI_{50} among all actual activities.

Single Dose Pharmacokinetic Evaluation. The single dose pharmacokinetic evaluation was carried out by Rosetta Pharmamate Co., Ltd., Taiwan. Compound **8c** was dissolved in polyethylene glycol 400/ethanol/water (30/5/65, v/v/v) to make the dosing solution of 0.2 mg/mL for intravenous administration. For oral dosing, **8c** was suspended in 0.5% methylcellulose (MC)/water to make a dosing suspension of 2 mg/mL.

Male CD-1 (Crl.) mice (body weight, 22−24 g) were used in this study. The source of animals was BioLasco Taiwan. Water was provided ad libitum, regardless of administration route. For intravenous administration, **8c** was administered via tail vein with a bolus dosing volume of 0.22−0.24 mL per animal (10 mL/kg). For oral dosing, the drug suspension was given via oral gavage with a dosing volume of 0.22−0.24 mL per animal (10 mL/kg). The animals were fasted for 4 h prior to oral administration and allowed standard chow 4 h after dosing.

Each blood sample (0.5 mL) was collected by cardiac puncture and collected in a 1.5 mL Eppendorf safe-lock microcentrifuge tube containing anticoagulant K-EDTA, followed by centrifugation (1.50 g, 4 °C) for 15 min. The plasma fraction was transferred to a clean microcentrifuge tube and stored at −20 °C for further analysis. The sampling time points were 0, 2, 5, 15, and 30 min and 1, 1.5, 2, 4, 6, 9, 24, and 27 h after intravenous dosing. For oral administration, the blood samples were collected at predose, 15 and 30 min, and 1, 1.5, 2, 4, 6, 9, 24, and 27 h after dosing. Three mice were used per time point.

The plasma concentrations of **8c** were measured by LC−MS/MS (Waters 2795 LC and Micromass Quattro Ultima) method with a reversed-phase Biosil ODS column. The plasma samples were mixed with acetonitrile and centrifuged, and the supernatant was injected onto an LC column. The pharmacokinetic parameters were calculated from mean plasma concentrations by WinNonlin Standard program (version 3.1, Pharsight Corp) [Rosetta Pharmamate Co., Ltd.].

Assessment of Toxicity. Mice (BALB/c) were handled in accordance with the National Science Council Guideline of Taiwan. The procedure of the animal model was approved by Animal Facility Care in Kaohsiung Medical University, Taiwan. The mice were randomly grouped on the basis of the body weight using the stratified randomization method. The number of mice was 3 in each group. Compound **8c** was dissolved in polyethylene glycol 400/ethanol/water, 20/20/60, v/v/v) and intravenously administered (10, 20, 40 mg/kg) into the tail vein of mice once every 3 days for 2 weeks. The mice were weighed during the experimental period. The blood was collected from the heart in mice under anesthesia with ether after fasting for 24 h as previously reported.[70] Glutamic oxaloacetic transaminase (GOT), glutamic pyruvate transaminase (GPT), blood urea nitrogen (BUN), and creatinine were measured using a Beckman LX-20 analyzer. Organs (liver and kidney) were collected after anatomizing the mice. Organs of tissues were stained with H&E stain and examined microscopically.

Acknowledgment. Financial support of this work by the National Science Council of the Republic of China is gratefully acknowledged. We also thank National Cancer Institute (NCI) of the U.S. for the anticancer screenings and the National Center for High-Performance Computing for providing computer resources and chemical database services.

Supporting Information Available: Information about the X-ray crystallography of **5a**. This material is available free of charge via the Internet at http://pubs.acs.org.

References

(1) Coban, G.; Zencir, S.; Zupko, I.; Rethy, B.; Gunes, H. S.; Topcu, Z. Synthesis and biological activity evaluation of 1*H*-benzimidazoles via mammalian DNA topoisomerase I and cytostaticity assays. *Eur. J. Med. Chem.* **2009**, *44*, 2280–2285.
(2) Feng, W.; Satyanarayana, M.; Tsai, Y.-C.; Liu, A. A.; Liu, L. F.; LaVoie, E. J. 12-Substituted 2,3-dimethoxy-8,9-methylenedioxybenzo[*f*]phenanthridines as novel topoisomerase I-targeting antitumor agents. *Bioorg. Med. Chem.* **2009**, *17*, 2877–2885.
(3) Sunami, S.; Nishimura, T.; Nishimura, I.; Ito, S.; Arakawa, H.; Ohkubo, M. Synthesis and biological activities of topoisomerase I inhibitors, 6-arylmethylamino analogues of edotecarin. *J. Med. Chem.* **2009**, *52*, 3225–3237.
(4) Feng, W.; Satyanarayana, M.; Tsai, Y.-C.; Liu, A. A.; Liu, L. F.; La, V.; Edmond, J. Novel topoisomerase I-targeting antitumor agents synthesized from the *N*,*N*,*N*-trimethylammonium derivative of ARC-111, 5*H*-2,3-dimethoxy-8,9-methylenedioxy-5-[(2-*N*,*N*,*N*-trimethylammonium)ethyl]dibenzo[*c*,*h*][1,6]naphthyridin-6-one iodide. *Eur. J. Med. Chem.* **2009**, *44*, 3433–3438.
(5) You, Q.-D.; Li, Z.-Y.; Huang, C.-H.; Yang, Q.; Wang, X.-J.; Guo, Q.-L.; Chen, X.-G.; He, X.-G.; Li, T.-K.; Chern, J.-W. Discovery of a novel series of quinolone and naphthyridine derivatives as potential topoisomerase I inhibitors by scaffold modification. *J. Med. Chem.* **2009**, *52*, 5649–5661.
(6) Diwan, R.; Malpathak, N. Furanocoumarins: novel topoisomerase I inhibitors from *Ruta graveolens* L. *Bioorg. Med. Chem.* **2009**, *17*, 7052–7055.
(7) Cinelli, M. A.; Cordero, B.; Dexheimer, T. S.; Pommier, Y.; Cushman, M. Synthesis and biological evaluation of 14-(aminoalkyl-aminomethyl)aromathecins as topoisomerase I inhibitors: investigating the hypothesis of shared structure−activity relationships. *Bioorg. Med. Chem.* **2009**, *17*, 7145–7155.
(8) Song, Y.; Shao, Z.; Dexheimer, T. S.; Scher, E. S.; Pommier, Y.; Cushman, M. Structure-based design, synthesis, and biological studies of new anticancer norindenoisoquinoline topoisomerase I inhibitors. *J. Med. Chem.* **2010**, *53*, 1979–1989.
(9) Guo, W.; Miao, Z.; Sheng, C.; Yao, J.; Feng, H.; Zhang, W.; Zhu, L.; Liu, W.; Cheng, P.; Zhang, J.; Che, X.; Wang, W.; Luo, C.; Xu, Y. Synthesis and evaluation of 9-benzylideneamino derivatives of homocamptothecin as potent inhibitors of DNA topoisomerase I. *Eur. J. Med. Chem.* **2010**, *45*, 2223–2228.
(10) Loza-Mejia, M. A.; Olvera-Vazquez, S.; Maldonado-Hernandez, K.; Guadarrama-Salgado, T.; Gonzalez-Sanchez, I.; Rodriguez-Hernandez, F.; Solano, J. D.; Rodriguez-Sotres, R.; Lira-Rocha, A. Synthesis, cytotoxic activity, DNA topoisomerase-II inhibition, molecular modeling and structure−activity relationship of 9-anilinothiazolo[5,4-*b*]quinoline derivatives. *Bioorg. Med. Chem.* **2009**, *17*, 3266–3277.
(11) Ryckebusch, A.; Garcin, D.; Lansiaux, A.; Goossens, J.-F.; Baldeyrou, B.; Houssin, R.; Bailly, C.; Hénichart., J.-P. Synthesis,

cytotoxicity, DNA interaction, and topoisomerase II inhibition properties of novel indeno[2,1-*c*]quinolin-7-one and indeno-[1,2-*c*]isoquinolin-5,11-dione derivatives. *J. Med. Chem.* **2008**, *51*, 3617–3629.
(12) Sperry, J.; Lorenzo-Castrillejo, I.; Brimble, M. A.; Machin, F. Pyranonaphthoquinone derivatives of eleutherin, ventiloquinone L, thysanone and nanaomycin A possessing a diverse topoisomerase II inhibition and cytotoxicity spectrum. *Bioorg. Med. Chem.* **2009**, *17*, 7131–7137.
(13) Chen, Z.; Liang, X.; Zhang, H.; Xie, H.; Liu, J.; Xu, Y.; Zhu, W.; Wang, Y.; Wang, X.; Tan, S.; Kuang, D.; Qian, X. A new class of naphthalimide-based antitumor agents that inhibit topoisomerase II and induce lysosomal membrane permeabilization and apoptosis. *J. Med. Chem.* **2010**, *53*, 2589–2600.
(14) Huang, H.; Chen, Q.; Xin, K.; Meng, L.; Lin, L.; Wang, X.; Zhu, C.; Wang, Y.; Chen, Z.; Li, M.; Jiang, H.; Chen, K.; Ding, J.; Liu, H. A series of α-heterocyclic carboxaldehyde thiosemicarbazones inhibit topoisomerase IIα catalytic activity. *J. Med. Chem.* **2010**, *53*, 3048–3064.
(15) Leon, L. G.; Rios-Luci, C.; Tejedor, D.; Perez-Roth, E.; Montero, J. C.; Pandiella, A.; Garcia-Tellado, F.; Padron, J. M. Mitotic arrest induced by a novel family of DNA topoisomerase II inhibitors. *J. Med. Chem.* **2010**, *53*, 3835–3839.
(16) Rao, V. A.; Agama, K.; Holbeck, S.; Pommier, Y. Batracylin (NSC 320846), a dual inhibitor of DNA topoisomerases I and II induces histone γ-H2AX as a biomarker of DNA damage. *Cancer Res.* **2007**, *67*, 9971–9979.
(17) Wang, S.; Miller, W.; Milton, J.; Vicker, N.; Stewart, A.; Charlton, P.; Mistry, P.; Hardick, D.; Denny, W. A. Structure−activity relationships for analogues of the phenazine-based dual topoisomerase I/II inhibitor XR11576. *Bioorg. Med. Chem. Lett.* **2002**, *12*, 415–418.
(18) Vicker, N.; Burgess, L.; Chuckowree, I. S.; Dodd, R.; Folkes, A. J.; Hardick, D. J.; Hancox, T. C.; Miller, W.; Milton, J.; Sohal, S.; Wang, S.; Wren, S. P.; Charlton, P. A.; Dangerfield, W.; Liddle, C.; Mistry, P.; Stewart, A. J.; Denny, W. A. Novel angular benzophenazines: dual topoisomerase I and topoisomerase II inhibitors as potential anticancer agents. *J. Med. Chem.* **2002**, *45*, 721–739.
(19) Perrin, D.; van Hille, B.; Barret, J.-M.; Kruczynski, A.; Etievant, C.; Imbert, T.; Hill, B. T. F 11782, a novel epipodophylloid non-intercalating dual catalytic inhibitor of topoisomerases I and II with an original mechanism of action. *Biochem. Pharmacol.* **2000**, *59*, 807–819.
(20) Karki, R.; Thapa, P.; Kang, M. J.; Jeong, T. C.; Nam, J. M.; Kim, H.-L.; Na, Y.; Cho, W.-J.; Kwon, Y.; Lee, E.-S. Synthesis, topoisomerase I and II inhibitory activity, cytotoxicity, and structure−activity relationship study of hydroxylated 2,4-diphenyl-6-aryl pyridines. *Bioorg. Med. Chem.* **2010**, *18*, 3066–3077.
(21) Thapa, P.; Karki, R.; Choi, H.; Choi, J. H.; Yun, M.; Jeong, B.-S.; Jung, M.-J.; Nam, J. M.; Na, Y.; Cho, W.-J.; Kwon, Y.; Lee, E.-S. Synthesis of 2-(thienyl-2-yl or -3-yl)-4-furyl-6-aryl pyridine derivatives and evaluation of their topoisomerase I and II inhibitory activity, cytotoxicity, and structure−activity relationship. *Bioorg. Med. Chem.* **2010**, *18*, 2245–2254.
(22) Van, G., R.; Lendfers, R. R. H.; Schellens, J. H. M.; Bult, A.; Beijnen, J. H. Dual topoisomerase I/II inhibitors. *J. Oncol. Pharm. Pract.* **2000**, *6*, 92–108.
(23) Atwell, G. J.; Cain, B. F.; Seelye, R. N. Potential antitumor agents. 12. 9-Anilinoacridines. *J. Med. Chem.* **1972**, *15*, 611–615.
(24) Gamage, S. A.; Tepsiri, N.; Wilairat, P.; Wojcik, S. J.; Figgitt, D. P.; Ralph, R. K.; Denny, W. A. Synthesis and in vitro evaluation of 9-anilino-3,6-diaminoacridines active against a multidrug-resistant strain of the malaria parasite *Plasmodium falciparum*. *J. Med. Chem.* **1994**, *37*, 1486–1494.
(25) Gamage, S. A.; Figgitt, D. P.; Wojcik, S. J.; Ralph, R. K.; Ransijn, A.; Mauel, J.; Yardley, V.; Snowdon, D.; Croft, S. L.; Denny, W. A. Structure−activity relationships for the antileishmanial and antitrypanosomal activities of 1′-substituted 9-anilinoacridines. *J. Med. Chem.* **1997**, *40*, 2634–2642.
(26) Stanslas, J.; Hagan, D. J.; Ellis, M. J.; Turner, C.; Carmichael, J.; Ward, W.; Hammonds, T. R.; Stevens, M. F. Antitumor polycyclic acridines. 7. Synthesis and biological properties of DNA affinic tetra- and pentacyclic acridines. *J. Med. Chem.* **2000**, *43*, 1563–1572.
(27) Su, T. L.; Chou, T. C.; Kim, J. Y.; Huang, J. T.; Ciszewska, G.; Ren, W. Y.; Otter, G. M.; Sirotnak, F. M.; Watanabe, K. A. 9-Substituted acridine derivatives with long half-life and potent antitumor activity: synthesis and structure−activity relationships. *J. Med. Chem.* **1995**, *38*, 3226–3235.
(28) Atwell, G. J.; Baguley, B. C.; Finlay, G. J.; Rewcastle, G. W.; Denny, W. A. Potential antitumor agents. 47. 3′-Methylamino analogues of amsacrine with in vivo solid tumor activity. *J. Med. Chem.* **1986**, *29*, 1769–1776.
(29) Chen, I. L.; Chen, Y. L.; Tzeng, C. C.; Chen, I. S. Synthesis and cytotoxic evaluation of some 4-anilinofuro[2,3-*b*]quinoline derivatives. *Helv. Chim. Acta* **2002**, *85*, 2214–2221.
(30) Chen, I. L.; Chen, Y. L.; Tzeng, C. C. An efficient synthesis of antitumor 4-anilinofuro[2,3-*b*]quinoline derivatives. *Chin. Pharm. J.* **2003**, *55*, 49–53.
(31) Chen, Y. L.; Chen, I. L.; Wang, T. C.; Han, C. H.; Tzeng, C. C. Synthesis and anticancer evaluation of certain 4-anilinofuro-[2,3-*b*]quinoline and 4-anilinofuro[3,2-*c*]quinoline derivatives. *Eur. J. Med. Chem.* **2005**, *40*, 928–934.
(32) Zhao, Y. L.; Chen, Y. L.; Tzeng, C. C.; Chen, I. L.; Wang, T. C.; Han, C. H. Synthesis and cytotoxic evaluation of certain 4-(phenylamino)furo[2,3-*b*]quinoline and 2-(furan-2-yl)-4-(phenyl-amino)-quinoline derivatives. *Chem. Biodiversity* **2005**, *2*, 205–214.
(33) Huang, Y. T.; Huang, D. M.; Guh, J. H.; Chen, I. L.; Tzeng, C. C.; Teng, C. M. CIL-102 interacts with microtubule polymerization and causes mitotic arrest following apoptosis in the human prostate cancer PC-3 cell line. *J. Biol. Chem.* **2005**, *280*, 2771–2779.
(34) Chen, Y. L.; Lin, H. C.; Yang, C. N.; Lu, P. J.; Tzeng, C. C. Synthesis and antiproliferative evaluation of 4-anilino-*n*-methoxyfuro[2,3-*b*]quinoline derivatives. *Chem. Biodiversity* **2008**, *4*, 267–278.
(35) Alvarez-Ibarra, C.; Fernández-Granda, R.; Quiroga, M. L.; Carbonell, A.; Cárdenas, F.; Giralt, E. Synthesis and antitumor evaluation of new thiazolo[5,4-*b*]quinoline derivatives. *J. Med. Chem.* **1997**, *40*, 668–676.
(36) Rodríguez-Loaiza, P.; Quintero, A.; Rodríguez-Sotres, R.; Solano, J. D.; Lira-Rocha, A. Synthesis and evaluation of 9-anilinothiazolo-[5,4-*b*]quinoline derivatives as potential antitumorals. *Eur. J. Med. Chem.* **2004**, *39*, 5–10.
(37) Wall, M. E.; Wani, M. C.; Cook, C. E.; Palmer, K. H.; McPhail, A. T.; Sim, G. A. Plant antitumor agents. I. The isolation and structure of camptothecin, a novel alkaloid leukemia and tumor inhibitor from *Camptotheca acuminates*. *J. Am. Chem. Soc.* **1966**, *88*, 3888–3890.
(38) Werbovetz, K. A.; Bhattacharjee, A. K.; Brendle, J. J.; Scovill, J. P. Analysis of stereoelectronic properties of camptothecin analogues in relation to biological activity. *Bioorg. Med. Chem.* **2000**, *8*, 1741–1747.
(39) Burke, T. G.; Mi, Z. The structural basis of camptothecin interactions with human serum albumin: impact on drug stability. *J. Med. Chem.* **1994**, *37*, 40–46.
(40) Fox, B. M.; Xiao, X.; Antony, S.; Kohlhagen, G.; Pommier, Y.; Staker, B. L.; Stewart, L.; Cushman, M. Design, synthesis, and biological evaluation of cytotoxic 11-alkenylindenoisoquinoline topoisomerase I inhibitors and indenoisoquinoline-camptothecin hybrids. *J. Med. Chem.* **2003**, *46*, 3275–3282.
(41) Kohlhagen, G.; Paull, K.; Cushman, M.; Nagafuji, P.; Pommier, Y. Protein-linked DNA strand breaks induced by NSC 314622, a novel noncamptothecin topoisomerase I poison. *Mol. Pharmacol.* **1998**, *54*, 50–58.
(42) Antony, S.; Jayaraman, M.; Laco, G.; Kohlhagen, G.; Kohn, K. W.; Cushman, M.; Pommier, Y. Differential induction of topoisomerase I-DNA cleavage complexes by the indenoisoquinoline MJ-III-65 (NSC 706744) and camptothecin: base sequence analysis and activity against camptothecin-resistant topoisomerases I. *Cancer Res.* **2003**, *63*, 7428–7435.
(43) Cushman, M.; Jayaraman, M.; Vroman, J. A.; Fukunaga, A. K.; Fox, B. M.; Kohlhagen, G.; Strumberg, D.; Pommier, Y. Synthesis of new indeno[1,2-*c*]isoquinolines: cytotoxic non-camptothecin topoisomerase I inhibitors. *J. Med. Chem.* **2000**, *43*, 3688–3698.
(44) Jayaraman, M.; Fox, B. M.; Hollingshead, M.; Kohlhagen, G.; Pommier, Y.; Cushman, M. Synthesis of new dihydroindeno[1,2-*c*]isoquinoline and indenoisoquinolinium chloride topoisomerase I inhibitors having high in vivo anticancer activity in the hollow fiber animal model. *J. Med. Chem.* **2002**, *45*, 242–249.
(45) Nagarajan, M.; Xiao, X.; Antony, S.; Kohlhagen, G.; Pommier, Y.; Cushman, M. Design, synthesis, and biological evaluation of indenoisoquinoline topoisomerase I inhibitors featuring polyamine side chains on the lactam nitrogen. *J. Med. Chem.* **2003**, *46*, 5712–5724.
(46) Staker, B. L.; Feese, M. D.; Cushman, M.; Pommier, Y.; Zembower, D.; Stewart, L.; Burgin, A. B. Structures of three classes of anticancer agents bound to the human topoisomerase I-DNA covalent complex. *J. Med. Chem.* **2005**, *48*, 2336–2345.
(47) Hsiang, Y. H.; Hertzberg, R.; Hecht, S.; Liu, L. F. Camptothecin induces protein-linked DNA breaks via mammalian DNA topoisomerase I. *J. Biol. Chem.* **1985**, *260*, 14873–14878.
(48) Hertzberg, R. P.; Caranfa, M. J.; Hecht, S. M. On the mechanism of topoisomerase I inhibition by camptothecin: evidence for

binding to an enzyme-DNA complex. *Biochemistry* **1989**, *28*, 4629–4638.
(49) Stewart, L.; Redinbo, M. R.; Qiu, X.; Hol, W. G.; Champoux, J. J. A model for the mechanism of human topoisomerase I. *Science* **1998**, *279*, 1534–1541.
(50) Deady, L. W.; Desneves, J.; Kaye, A. J.; Finlay, G. J.; Baguley, B. C.; Denny, W. A. Positioning of the carboxamide side chain in 11-oxo-11*H*-indeno[1,2-*b*]quinolinecarboxamide anticancer agents: effects on cytotoxicity. *Bioorg. Med. Chem.* **2001**, *9*, 445–452.
(51) Asao, T.; Okazaki, S.; Wakita, S.; Utsuki, T.; Yamada, Y. Preparation of Indenoquinoline Derivatives and Analogs as Antitumor Agents. JP 09143166 A2, 1997.
(52) Malecki, N.; Carato, P.; Rigo, B.; Goossens, J. F.; Houssin, R.; Bailly, C.; Hénichart, J. P. Synthesis of condensed quinolines and quinazolines as DNA ligands. *Bioorg. Med. Chem.* **2004**, *12*, 641–647.
(53) Padget, K.; Stewart, A.; Charlton, P.; Tilby, M. J.; Austin, C. A. An investigation into the formation of *N*-[2-(dimethylamino)ethyl]-acridine-4-carboxamide (DACA) and 6-[2-(dimethylamino)ethylamino]-3-hydroxy-7*H*-indeno[2,1-*c*]quinolin-7-one dihydrochloride (TAS-103) stabilised DNA topoisomerase I and II cleavable complexes in human leukaemia cells. *Biochem. Pharmacol.* **2000**, *60*, 817–821.
(54) Utsugi, T.; Aoyagi, K.; Asao, T.; Okazaki, S.; Aoyagi, Y.; Sano, M.; Wierzba, K.; Yamada, Y. Antitumor activity of a novel quinoline derivative, TAS-103, with inhibitory effects on topoisomerases I and II. *Jpn. J. Cancer Res.* **1997**, *88*, 992–1002.
(55) Aoyagi, Y.; Kobunai, T.; Utsugi, T.; Oh-hara, T.; Yamada, Y. In vitro antitumor activity of TAS-103, a novel quinoline derivative that targets topoisomerases I and II. *Jpn. J. Cancer Res.* **1999**, *90*, 578–587.
(56) Ishida, K.; Asao, T. Self-association and unique DNA binding properties of the anti-cancer agent TAS-103, a dual inhibitor of topoisomerases I and II. *Biochim. Biophys. Acta* **2002**, *1587*, 155–163.
(57) Chen, Y. L.; Hung, H. M.; Lu, C. M.; Li, K. C.; Tzeng, C. C. Synthesis and anticancer evaluation of certain indolo[2,3-*b*]quinoline derivatives. *Bioorg. Med. Chem.* **2004**, *12*, 6539–6546.
(58) Lu, C. M.; Chen, Y. L.; Chen, H. L.; Chen, C. A.; Lu, P. J.; Yang, C. N.; Tzeng, C. C. Synthesis and antiproliferative evaluation of certain indolo[3,2-*c*]quinoline derivatives. *Bioorg. Med. Chem.* **2010**, *18*, 1948–1957.
(59) Tseng, C. H.; Chen, Y. L.; Lu, P. J.; Yang, C. N.; Tzeng, C. C. Synthesis and antiproliferative evaluation of certain indeno[1,2-*c*]-quinoline derivatives. *Bioorg. Med. Chem.* **2008**, *15*, 3151–3162.
(60) Tseng, C. H.; Chen, Y. L.; Chung, K. Y.; Cheng, C. M.; Wang, C. H.; Tzeng, C. C. Synthesis and antiproliferative evaluation of 6-arylindeno[1,2-*c*]quinoline derivatives. *Bioorg. Med. Chem.* **2009**, *17*, 7465–7476.
(61) Cerri, A.; Almirante, N.; Barassi, P.; Benicchio, A.; Fedrizzi, G.; Ferrari, P.; Micheletti, R.; Quadri, L.; Ragg, E.; Rossi, E.; Santagostino, M.; Schiavone, A.; Serra, F.; Zappavigna, M. P.; Melloni, P. 17β-*O*-Aminoalkyloximes of 5β-androstane-3β,14β-diol with digitalis-like activity: synthesis, cardiotonic activity, structure−activity relationships, and molecular modeling of the Na^+,K^+-ATPase receptor. *J. Med. Chem.* **2000**, *43*, 2332–2349.
(62) Shearman, M. S.; Ragan, C. I.; Iversen, L. L. Inhibition of PC12 cell redox activity is a specific, early indicator of the mechanism of beta-amyloid-mediated cell death. *Proc. Natl. Acad. Sci. U.S.A.* **1994**, *91*, 1470–1474.
(63) Chowdhury, A. R.; Sharma, S.; Mandal, S.; Goswami, A.; Mukhopadhyay, S.; Majumder, H. K. Luteolin, an emerging anticancer flavonoid, poisons eukaryotic DNA topoisomerase I. *Biochem. J.* **2002**, *366*, 653–661.
(64) Gillson, B. S; Ross, W. E. DNA topoisomerase II: a primer on the enzyme and its unique role as a multidrug target in cancer chemotherapy. *Pharmacol. Ther.* **1987**, *32*, 89–106.
(65) Lu, P. J.; Zhou, X. Z.; Liou, Y. C.; Noel, J. P.; Lu, K. P. Critical role of WW domain phosphorylation in regulating phosphoserine binding activity and pin1 function. *J. Biol. Chem.* **2002**, *277*, 2381–2384.
(66) Lin, Y. T.; Liang, L. C.; Ko, C. Y.; Lo, Y. K.; Cheng, J. T.; Lu, P. J. The binding and phosphorylation of Thr231 is critical for Tau's hyperphosphorylation and functional regulation by glycogen synthase kinase 3β. *J. Neurochem.* **2007**, *130*, 802–813.
(67) Akar, U.; Ozpolat, B.; Mehta, K.; Lopez-Berestein, G.; Zhang, D.; Ueno, N. T.; Hortobagyi, G. N.; Arun, B. Targeting p70S6K prevented lung metastasis in a breast cancer xenograft model. *Mol. Cancer Ther.* **2010**, *9*, 1180–1187.
(68) Cramer, R. D., III; Patterson, D. E.; Bunce, J. D. Comparative molecular field analysis (CoMFA). 1. Effect of shape on binding of steroid to carrier proteins. *J. Am. Chem. Soc.* **1988**, *110*, 5959–5967.
(69) Leevy, W. M.; Weber, M. E.; Gokel, M. R.; Hughes-Stranger, G. B.; Daranciang, D. D.; Ferdani, R.; Gokel, G. W. Correlation of bilayer membrane cation transport and biological activity in alkyl-substituted lariat ethers. *Org. Biomol. Chem.* **2005**, *3*, 1647–1652.
(70) Aiso, S.; Arito, H.; Nishizawa, T.; Nagano, K.; Yamamoto, S.; Matsushima, T. Thirteen-week inhalation toxicity of *p*-dichlorobenzene in mice and rats. *J. Occup. Health* **2005**, *47*, 249–260.